Eigenstructure Techniques for 2-D Angle Estimation with Uniform Circular Arrays

Cherian P. Mathews, *Member, IEEE*, and Michael D. Zoltowski, *Member, IEEE*

Abstract— **The problem of 2-D angle estimation (azimuth and elevation) of multiple plane waves incident on a uniform circular array (UCA) of antennas is considered in this paper. Two eigenstructure-based estimation algorithms that operate in beamspace and employ phase mode excitation-based beamformers have been developed. The first, UCA-RB-MUSIC, is a beamspace version of MUSIC that offers numerous advantages over element space operation, including reduced computation, as subspace estimates are obtained via real-valued eigendecompositions, enhanced performance in correlated source scenarios due to the attendant forward-backward averaging effect, and the applicability of Root-MUSIC. The second, UCA-ESPRIT, represents a significant advance in the area of 2-D angle estimation. It is a novel *closed-form* algorithm that provides automatically paired source azimuth and elevation estimates. With UCA-ESPRIT, the eigenvalues of a matrix have the form $\mu_i = \sin\theta_i e^{j\phi_i}$, where θ_i and ϕ_i are the elevation and azimuth angles, respectively. Expensive search procedures being thus avoided, UCA-ESPRIT is superior to existing 2-D angle estimation algorithms with respect to computational complexity. Finally, asymptotic expressions for the variances of the element space MUSIC and UCA-RB-MUSIC estimators for the 2-D scenario have been derived. Results of simulations that compare UCA-RB-MUSIC and UCA-ESPRIT and also validate the theoretical performance expressions are presented.**

I. Introduction

ESTIMATING the directions of arrival (DOA's) of propagating plane waves is a problem of interest in a variety of applications, including radar, mobile communications, sonar, and seismology. The widely studied uniform linear array (ULA) can provide estimates of source bearings relative to the array axis. However, a planar array is required if estimates of source azimuth and elevation are required. The following properties of uniform circular arrays (UCA's) make them attractive in the context of DOA estimation. UCA's provide 360° azimuthal coverage and also provide information on source elevation angles. In addition, directional patterns synthesized with UCA's can be electronically rotated in the plane of the array without significant change of beam shape. ULA's, in contrast, provide only 180° coverage, and beams formed with ULA's broaden as the array is steered away from boresight. Phase mode excitation of UCA's, which essentially is Fourier analysis of the array excitation function, was studied by researchers in the early 1960's [1], [2]. This theory led to a powerful pattern synthesis technique for UCA's [3]. Davies [4] also showed how the simple phasing techniques normally associated with ULA's (Butler beamforming matrices) could be used to provide the necessary phasing for pattern rotation with UCA's. These attractive features led to the development of experimental systems that employed phase mode excitation for pattern synthesis with UCA's [4], [5]. These systems, however, employed the beamforming principle to obtain DOA estimates; it is well known that beamforming cannot resolve closely spaced sources (spacing less than the main-lobe width of the array pattern). Two algorithms for DOA estimation with UCA's are developed in this paper. Both of them employ phase mode excitation-based beamforming in conjunction with subspace techniques to obtain high resolution DOA estimates. The first algorithm, UCA-RB (Real Beamspace) MUSIC, is a beamspace version of the popular MUSIC algorithm [6], wherein the beamspace manifold is *real-valued*, thereby facilitating real-valued matrix-based computations. The second algorithm is coined UCA-ESPRIT because the steps involved in the algorithm are similar to those of TLS-ESPRIT [7]. The applicability of the ESPRIT principle in conjunction with rotationally invariant arrays (such as UCA's) was studied in [8]. It was shown that such techniques cannot provide unique DOA estimates when more than one source is present. Although this is true in element space, the phase mode excitation-based transformation to beamspace induces a beamspace manifold whose structure can be exploited to develop the ESPRIT-like algorithm UCA-ESPRIT.

Phase mode excitation-based beamforming synthesizes a beamspace manifold similar to that of a ULA, with azimuthal variation being through a centro-Hermitian vector [9], and with a symmetric amplitude taper dependent on the elevation angle. This structure is the basis for the development of the UCA-RB-MUSIC algorithm that requires only *real-valued* eigenvalue decompositions (EVD's) to obtain signal and noise subspace estimates. UCA-RB-MUSIC offers other advantages, such as improved estimator performance in correlated source scenarios due to an inherent forward/backward (FB) average, and the ability to employ Root-MUSIC to obtain azimuth estimates of sources at a given elevation. The algorithm does require a 2-D spectral search to obtain DOA estimates. The computational complexity is, however, lower than for element space MUSIC, as samples of the 2-D beamspace MUSIC spectrum corresponding to a given elevation can be obtained via an FFT. Element space MUSIC also requires complex-valued EVD's for subspace estimates, and ULA techniques such as Root-MUSIC cannot be employed. Averaging similar

Manuscript received May 1, 1993; revised January 10, 1994. This work was supported by AFOSR under contract no. F49620-92-J-0198 in conjunction with Wright Laboratories. The associate editor coordinating the review of this paper and approving it for publication was Prof. John Goutsias.

The authors are with the School of Electrical Engineering, Purdue University, West Lafayette, IN 47907–1285 USA.

IEEE Log Number 9403266.

to FB averaging can be performed in element space with UCA's, but only when the number N of array elements is even. It was shown in [10] that the asymptotic performance of a beamspace MUSIC estimator can never be superior to that of the corresponding element space MUSIC estimator. While this is generally true, UCA-RB-MUSIC can *outperform* element space MUSIC in correlated source scenarios when N is odd. This is due to the decorrelating effect of the FB average inherent in UCA-RB-MUSIC, but not available in element space for odd N. Previous research efforts on the application of ULA techniques with UCA's are surveyed in Section III. Comparisons between these techniques and UCA-RB-MUSIC are also made.

The ESPRIT [7] principle has been employed by several researchers [11], [12] for azimuth and elevation estimation with planar arrays. The UCA-ESPRIT algorithm is fundamentally different from ESPRIT in that the UCA does not possess the displacement invariances required by ESPRIT-based algorithms. The similarity to ESPRIT is in that the eigenvalues of a matrix (that is derived from the least squares solution to an overdetermined system of equations) directly yield the DOA estimates. The eigenvalues have the form $\mu_i = \sin\theta_i e^{j\phi_i}$, where θ_i and ϕ_i are the elevation and azimuth angles of the ith source, respectively. The algorithm thus has the novel feature that the eigenvalues yield *automatically paired* azimuth and elevation estimates. Another similarity with ESPRIT is that the algorithm can resolve only about half the number of sources that UCA-RB-MUSIC can. UCA-ESPRIT represents a significant advance in the area of 2-D arrival angle estimation. To our knowledge, it is the only "closed-form" algorithm yielding the azimuth and elevation of each source automatically paired. The term *closed-form* connotes that the algorithm does not require a 2-D spectral search as with MUSIC [6], or iterative optimization procedures as in [12] and [13]. The algorithm also dispenses with the need for pairing independently obtained azimuth and elevation estimates as in [11]. UCA-ESPRIT is clearly superior to the above mentioned estimation techniques in terms of computational requirements. However, simulations reveal that the UCA-RB-MUSIC estimator has lower variance than the UCA-ESPRIT estimator. For improved estimator performance, the azimuth and elevation estimates from UCA-ESPRIT can be used as starting points for localized Newton searches of the 2-D UCA-RB-MUSIC spectrum.

Results on the asymptotic performance analysis of the MUSIC estimator are derived in [14] for the case where the MUSIC spectrum is a function of one variable. The MUSIC spectrum for planar arrays such as the UCA is a function of two variables, azimuth and elevation, and performance analysis results do not appear to be available for this case. We derive herein asymptotic expressions (applicable with arbitrary array configurations) for the variance of the MUSIC estimator, when the MUSIC spectrum is a function of both azimuth and elevation. Expressions for the asymptotic variance of the UCA-RB-MUSIC estimator are also derived. The performance analysis results are verified by computer simulations.

The outline of the paper is as follows. Section II provides the relevant background on phase mode excitation of circular arrays. This background leads to the development of the UCA-RB-MUSIC algorithm in Section III. The UCA-ESPRIT algorithm is next described in Section IV. The asymptotic performance analysis results alluded to earlier are presented in Section V. The results of computer simulations of the UCA-RB-MUSIC and UCA-ESPRIT algorithms are reported in Section VI. Finally, Section VII concludes the paper by summarizing the important points.

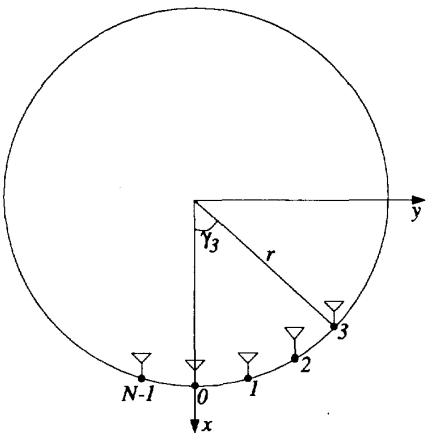

Fig. 1. Uniform circular array geometry.

II. Phase Mode Excitation for Circular Arrays

The UCA geometry is depicted in Fig. 1. The antenna elements, assumed to be identical and omnidirectional, are uniformly distributed over the circumference of a circle of radius r in the xy plane. A spherical coordinate system is used to represent the arrival directions of the incoming plane waves. The origin of the coordinate system is located at the center of the array. Source elevation angles $\theta \in [0, \pi/2]$ are measured down from the z axis, and azimuth angles $\phi \in [0, 2\pi]$ are measured counterclockwise from the x axis.

Element n of the array is displaced by an angle $\gamma_n = 2\pi n/N$ from the x axis. The position vector at this location is $\vec{p}_n = (r\cos\gamma_n, r\sin\gamma_n, 0)$. Consider a narrowband plane wave with wavenumber $k_0 = 2\pi/\lambda$ propagating in the direction $-\hat{r}$, with elevation and azimuth θ and ϕ, respectively. The unit vector $\hat{r}$ has Cartesian coordinates $\hat{r} = (\sin\theta\cos\phi, \sin\theta\sin\phi, \cos\theta)$. The phase difference between the complex envelopes of the signals received at the origin and at element n at a given time is $\psi_n = e^{jk_0\hat{r}\cdot\vec{p}_n} = e^{jk_0 r\sin\theta\cos(\phi-\gamma_n)} = e^{j\zeta\cos(\phi-\gamma_n)}$, where $\zeta = k_0 r\sin\theta$. The element space circular array manifold vector is therefore given by

$$\underline{\mathbf{a}}(\boldsymbol{\theta}) = \underline{\mathbf{a}}(\zeta,\phi) = \begin{bmatrix} e^{j\zeta\cos(\phi-\gamma_0)} \\ e^{j\zeta\cos(\phi-\gamma_1)} \\ \vdots \\ e^{j\zeta\cos(\phi-\gamma_{N-1})} \end{bmatrix} \tag{1}$$

where the elevation dependence is through the parameter ζ, and the vector $\theta = (\zeta, \phi)$ is used to represent source arrival directions.

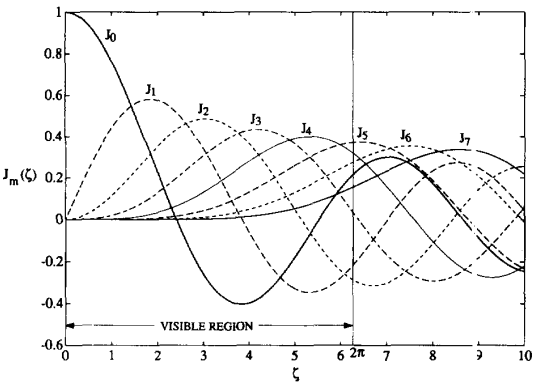

Fig. 2. Bessel functions.

A. Continuous Circular Aperture

Consider first the case of a continuous circular aperture. Any excitation function is periodic with period 2π and can hence be represented in terms of a Fourier series. The arbitrary excitation function $w(\gamma)$ thus has the representation $w(\gamma) = \sum_{m=-\infty}^{\infty} c_m e^{jm\gamma}$, where the mth phase mode $w_m(\gamma) = e^{jm\gamma}$ is just a spatial harmonic of the array excitation, and c_m is the corresponding Fourier series coefficient. The normalized far-field pattern resulting from exciting the aperture with the mth phase mode is $f_m^c(\boldsymbol{\theta}) = \frac{1}{2\pi}\int_0^{2\pi} w_m(\gamma) e^{j\zeta\cos(\phi-\gamma)} d\gamma$, where the superscript c denotes the continuous aperture. Substituting for $w_m(\gamma)$, the far-field pattern can be expressed as

$$f_m^c(\boldsymbol{\theta}) = j^m J_m(\zeta) e^{jm\phi} \tag{2}$$

where $J_m(\zeta)$ is the Bessel function of the first kind of order m. The far-field pattern has the same azimuthal variation $e^{jm\phi}$ as the excitation function itself. This property allows attractive directional patterns to be synthesized using phase mode excitation [3]. The amplitude and elevation dependence of the far-field pattern is through the Bessel function $J_m(\zeta)$. Consequently, only a limited number of modes can be excited by a given circular aperture. Let M denote the highest order mode that can be excited by the aperture at a reasonable strength. A rule of thumb for determining M is [3]

$$M \approx k_0 r. \tag{3}$$

This is justified as follows: The visible region $\theta \in [0, \pi/2]$ translates into $\zeta = k_0 r \sin\theta \in [0, k_0 r]$. M is chosen as above because the mode amplitude $J_m(\zeta)$ is small when the Bessel function order m exceeds its argument ζ. For mode orders $|m| \geq M$, $f_m^c(\boldsymbol{\theta})$ is small over the entire visible region. The beamformer for such a mode m thus severely attenuates sources from all directions.

To illustrate this property, consider a circular aperture of radius $r = \lambda$. Equation (3) suggests that the maximum mode order is $M = 6$ (the closest integer to 2π). The Bessel functions of order 0 through 7 are plotted in Fig. 2. The figure reveals that $J_7(\zeta)$ is indeed small over the entire visible region $0 \leq \zeta \leq 2\pi$. Thus, only phase modes of order $m \in [-6, 6]$ can be excited at a reasonable strength by the aperture.

B. Uniform Circular Array

We now consider phase mode excitation of an N element UCA. The normalized beamforming weight vector that excites the array with phase mode $m, |m| \leq M$ is

$$\begin{aligned}\mathbf{w}_m^H &= \frac{1}{N}[e^{jm\gamma_0}, e^{jm\gamma_1}, \ldots, e^{jm\gamma_{N-1}}] \\ &= \frac{1}{N}[1, e^{j2\pi m/N}, \ldots, e^{j2\pi m(N-1)/N}].\end{aligned} \tag{4}$$

The resulting array pattern $f_m^s(\boldsymbol{\theta})$, where the superscript s denotes the sampled aperture, is

$$f_m^s(\boldsymbol{\theta}) = \mathbf{w}_m^H \underline{\mathbf{a}}(\boldsymbol{\theta}) = \frac{1}{N}\sum_{n=0}^{N-1} e^{jm\gamma_n} e^{j\zeta\cos(\phi-\gamma_n)}. \tag{5}$$

For mode orders $|m| < N$, the array pattern can be expressed as [3]

$$\begin{aligned}f_m^s(\boldsymbol{\theta}) = j^m J_m(\zeta) e^{jm\phi} + \sum_{q=1}^{\infty} \big(&j^g J_g(\zeta) e^{-jg\phi} \\ &+ j^h J_h(\zeta) e^{jh\phi}\big)\end{aligned} \tag{6}$$

where $g = Nq - m$ and $h = Nq + m$. The first term in this equation, the principal term, is identical to the far-field pattern of (2) corresponding to the continuous aperture case. The remaining terms arise due to sampling of the continuous aperture, and are called residual terms. Examination of (6) reveals that the condition $N > 2|m|$ must be satisfied for the principal term to be the dominant one. The highest mode excited has order M, and we therefore need

$$N > 2M \tag{7}$$

array elements. This condition is identical to the Nyquist sampling criterion as M defines the maximum spatial frequency component in the array excitation. With $M = k_0 r$ as in (3), it is clear that (7) requires the circumferential spacing between adjacent array elements to be less than 0.5λ. Note that an interelement spacing of 0.5λ is sufficient to avoid grating lobes with ULA's.

The following discussion shows how the contribution of the residual terms to the pattern of (6) can be made as small as desired by choosing N appropriately. The residual term that contributes the most arises from the $q = 1$ index in (6), and its amplitude follows the Bessel function of order $N - |m|$. The residual contribution is clearly maximum for mode M, and the amplitude of this residual term follows $J_{N-M}(\zeta)$. Now, $J_{N-M}(\zeta)$ is monotone increasing over the visible region $[0, k_0 r]$ by virtue of the choice of M and N in (3) and (7). $J_{N-M}(k_0 r)$ is, therefore, an upper bound on the maximum contribution of any residual term. This upper bound can be made as small as desired by choosing a sufficiently large number N of array elements. We return to the example of the UCA of radius $r = \lambda$ and $M = 6$ to illustrate the selection of N. Equation 7 requires that the array have $N > 12$ elements. The upper bound on the maximum residual contribution $J_{N-M}(k_0 r)$ is tabulated in Table I for various values of N. The table indicates that the residual

TABLE I
MAXIMUM RESIDUAL CONTRIBUTION AS A FUNCTION OF N

N	13	14	15	16	17	18	19
$J_{N-M}(k_0r)$	0.158	0.073	0.029	0.010	0.003	8.8e-4	2.3e-4

contribution is "small enough" to be ignored for $N > 15$ elements (circumferential spacing $< 0.42\lambda$).

For the development of the UCA-RB-MUSIC and UCA-ESPRIT algorithms, we will assume that N has been chosen such that the residual terms are negligible for mode orders $|m| \leq M$. With the residual terms being ignored, the array patterns for the UCA are identical to those for continuous circular apertures, and are given by (2). Using the property $J_{-m}(\zeta) = (-1)^m J_m(\zeta)$ of Bessel functions, the UCA array pattern for mode m can be expressed as

$$f_m^s(\boldsymbol{\theta}) \approx j^{|m|} J_{|m|}(\zeta) e^{jm\phi} \quad |m| \leq M. \tag{8}$$

With this background on phase mode excitation of circular arrays, we now proceed to develop the UCA-RB (Real Beamspace) MUSIC algorithm.

III. REAL BEAMSPACE MUSIC FOR CIRCULAR ARRAYS

A. Beamforming Matrices and Manifold Vectors

The UCA-RB-MUSIC algorithm employs the beamformer $\mathbf{F}_{\mathbf{r}}^H$ to make the transformation from element space to beamspace. The beamspace transformation $\mathbf{F}_{\mathbf{r}}^H \underline{\mathbf{a}}(\boldsymbol{\theta}) = \mathbf{b}(\boldsymbol{\theta})$ maps the UCA manifold vector $\underline{\mathbf{a}}(\boldsymbol{\theta})$ of (1) onto the beamspace manifold $\mathbf{b}(\boldsymbol{\theta})$. The beamspace manifold $\mathbf{b}(\boldsymbol{\theta})$ is *real-valued* over the entire arrival angle space $\boldsymbol{\theta} = (\zeta, \phi) = (k_0 r \sin\theta, \phi)$, and this leads to the development of the UCA-RB-MUSIC algorithm that requires only real-valued matrix computations. The subscript $\mathbf{r}$ signifies that $\mathbf{F}_{\mathbf{r}}^H$ synthesizes a real-valued beamspace manifold, thereby facilitating Real Beamspace (RB) processing.

For clarity of description, we also introduce the beamformer $\mathbf{F}_{\mathbf{e}}^H$ that is based solely on the principle of phase mode excitation. This beamformer synthesizes the beamspace manifold $\mathbf{F}_{\mathbf{e}}^H \underline{\mathbf{a}}(\boldsymbol{\theta}) = \mathbf{a}_{\mathbf{e}}(\boldsymbol{\theta})$. The azimuthal variation of $\mathbf{a}_{\mathbf{e}}(\boldsymbol{\theta})$ is similar to that of a ULA and the elevation dependence takes the form of a symmetric amplitude taper. The beamspace manifold $\mathbf{a}_{\mathbf{e}}(\boldsymbol{\theta})$ is centro-Hermitian, and this immediately opens the avenue to real beamspace processing, as with ULA's [9]. Premultiplying $\mathbf{F}_{\mathbf{e}}^H$ by a matrix with centro-Hermitian rows clearly leads to a real-valued beamspace manifold. The beamformer $\mathbf{F}_{\mathbf{r}}^H$ is in fact defined in this fashion, with $\mathbf{F}_{\mathbf{r}}^H = \mathbf{W}^H \mathbf{F}_{\mathbf{e}}^H$, where the matrix $\mathbf{W}^H$ has centro-Hermitian rows. Both the beamformers $\mathbf{F}_{\mathbf{e}}^H$ and $\mathbf{F}_{\mathbf{r}}^H$ synthesize manifolds of size $M' = 2M + 1$. Equation (7), together with the need to suppress residual terms, makes the beamspace dimension a little lower than the element space dimension.

The beamforming matrix $\mathbf{F}_{\mathbf{e}}^H$ is defined by

$$\mathbf{F}_{\mathbf{e}}^H = \mathbf{C}_{\mathbf{v}} \mathbf{V}^H, \tag{9}$$

$$\text{where } \mathbf{C}_{\mathbf{v}} = \text{diag}\{j^{-M}, \ldots, j^{-1}, j^0, j^{-1}, \ldots, j^{-M}\} \tag{10}$$

$$\text{and } \mathbf{V} = \sqrt{N}[\mathbf{w}_{-M} \vdots \cdots \vdots \mathbf{w}_0 \vdots \cdots \vdots \mathbf{w}_M]. \tag{11}$$

The vector $\mathbf{w}_m^H$, defined in (4), excites the UCA with phase mode m, leading to a pattern of the form of (8). The term $j^{|m|}$ in (8) is cancelled by the corresponding term $j^{-|m|}$ in the matrix $\mathbf{C}_{\mathbf{v}}$. The beamspace manifold synthesized by $\mathbf{F}_{\mathbf{e}}^H$ is thus

$$\mathbf{a}_{\mathbf{e}}(\boldsymbol{\theta}) = \mathbf{F}_{\mathbf{e}}^H \underline{\mathbf{a}}(\boldsymbol{\theta}) = \mathbf{C}_{\mathbf{v}} \mathbf{V}^H \underline{\mathbf{a}}(\boldsymbol{\theta}) = \sqrt{N} \mathbf{J}_\zeta \mathbf{v}(\phi). \tag{12}$$

The azimuthal variation of $\mathbf{a}_{\mathbf{e}}(\boldsymbol{\theta})$ is through the vector

$$\mathbf{v}(\phi) = [e^{-jM\phi}, \ldots, e^{-j\phi}, e^{j0}, e^{j\phi}, \ldots, e^{jM\phi}]^T \tag{13}$$

that is similar in form to the ULA manifold vector. The elevation dependence takes the form of a symmetric amplitude taper through the matrix of Bessel functions

$$\mathbf{J}_\zeta = \text{diag}[J_M(\zeta), \ldots, J_1(\zeta), J_0(\zeta), J_1(\zeta), \ldots, J_M(\zeta)]. \tag{14}$$

The subscript $\mathbf{e}$ on $\mathbf{a}_{\mathbf{e}}(\boldsymbol{\theta})$ stands for "even," and is intended to reflect the fact that the diagonal elements of $\mathbf{J}_\zeta$ are even about the center element. This is in contrast to the manifold denoted $\mathbf{a}_{\mathbf{o}}(\boldsymbol{\theta})$ in Section IV. The beamspace manifold vectors are centro-Hermitian, satisfying $\tilde{\mathbf{I}}\mathbf{a}_{\mathbf{e}}(\boldsymbol{\theta}) = \mathbf{a}_{\mathbf{e}}^*(\boldsymbol{\theta})$, where $\tilde{\mathbf{I}}$ is the reverse permutation matrix with ones on the anti-diagonal and zeros elsewhere. It is easy to verify that the beamformer is orthogonal, satisfying $\mathbf{F}_{\mathbf{e}}^H \mathbf{F}_{\mathbf{e}} = \mathbf{I}$.

As stated earlier, the beamformer $\mathbf{F}_{\mathbf{r}}^H$ is constructed by premultiplying $\mathbf{F}_{\mathbf{e}}^H$ by a matrix $\mathbf{W}^H$ that has centro-Hermitian rows. The beamformer $\mathbf{F}_{\mathbf{r}}^H$ and the corresponding real-valued beamspace manifold $\mathbf{b}(\boldsymbol{\theta})$ are defined as follows:

$$\mathbf{F}_{\mathbf{r}}^H = \mathbf{W}^H \mathbf{F}_{\mathbf{e}}^H = \mathbf{W}^H \mathbf{C}_{\mathbf{v}} \mathbf{V}^H \tag{15}$$

$$\mathbf{b}(\boldsymbol{\theta}) = \mathbf{F}_{\mathbf{r}}^H \underline{\mathbf{a}}(\boldsymbol{\theta}) = \sqrt{N} \mathbf{W}^H \mathbf{J}_\zeta \mathbf{v}(\phi) \tag{16}$$

Any matrix satisfying $\tilde{\mathbf{I}}\mathbf{W} = \mathbf{W}^*$ yields a real-valued beamspace manifold $\mathbf{b}(\boldsymbol{\theta})$. We will construct $\mathbf{W}$ such that each row of $\mathbf{F}_{\mathbf{r}}^H$ synthesizes the same real-valued pattern, except for a rotation in azimuth, that is, $\mathbf{F}_{\mathbf{r}}^H$ synthesizes the $M' = 2M + 1$ beams $f(\zeta, \phi - \alpha_i)$, where $f(\zeta, \phi)$ is the basic beampattern. Here, $\alpha_i = 2\pi i / M', i \in [-M, M]$ are the azimuthal rotation angles. This choice of rotation angles makes $\mathbf{W}$ unitary, and $\mathbf{F}_{\mathbf{r}}^H$ is thus an orthogonal beamformer. We have

$$\mathbf{W} = \frac{1}{\sqrt{M'}}[\mathbf{v}(\alpha_{-M}) \vdots \cdots \vdots \mathbf{v}(\alpha_0) \vdots \cdots \vdots \mathbf{v}(\alpha_M)] \tag{17}$$

where $\mathbf{v}(\alpha)$ is defined in (13). With $\mathbf{W}$ as above, the basic beampattern is just the sum of the components of $\mathbf{a}_{\mathbf{e}}(\boldsymbol{\theta})$; we have $f(\zeta, \phi) = \sqrt{\frac{N}{M'}}\left[J_0(\zeta) + 2\sum_{m=1}^{M} J_m(\zeta)\cos(m\phi)\right]$. The beamformer $\mathbf{F}_{\mathbf{r}}^H$ thus synthesizes the $M' = 2M + 1$ dimensional real-valued beamspace manifold

$$\mathbf{b}(\boldsymbol{\theta}) = [f(\zeta, \phi - \alpha_{-M}), \ldots, f(\zeta, \phi - \alpha_{-1}), f(\zeta, \phi), f(\zeta, \phi - \alpha_1), \ldots, f(\zeta, \phi - \alpha_M)]^T. \tag{18}$$

B. The UCA-RB-MUSIC Algorithm

Invoking the standard data model for narrowband signals received by an antenna array, the array output vector at time t has the representation $\mathbf{x}(t) = \underline{\mathbf{A}}\mathbf{s}(t) + \mathbf{n}(t)$. Assuming d incident signals, $\underline{\mathbf{A}}$ is the $N \times d$ DOA matrix having the element space manifold vectors $\underline{\mathbf{a}}(\boldsymbol{\theta}_i)$ as its columns. The vector $\mathbf{s}(t)$ contains the signal complex envelopes at the array center, and $\mathbf{n}(t)$ is a vector of noise complex envelopes. The signals and the noises are assumed to be stationary, zero mean, uncorrelated random processes. The incident signals are assumed to be noncoherent, and the source covariance matrix $\mathbf{P} = \mathrm{E}[\mathbf{s}(t)\mathbf{s}^H(t)]$ is therefore positive definite. The noise process $\mathbf{n}(t)$ is assumed to be complex Gaussian distributed and spatially white with covariance matrix $\sigma\mathbf{I}$. Under these assumptions, the array output covariance matrix $\underline{\mathbf{R}} = \mathrm{E}[\mathbf{x}(t)\mathbf{x}^H(t)]$ has the form $\underline{\mathbf{R}} = \underline{\mathbf{A}}\mathbf{P}\underline{\mathbf{A}}^H + \sigma\mathbf{I}$.

The UCA-RB-MUSIC algorithm employs the beamformer $\mathbf{F}_\mathbf{r}^H$ to make the transformation from element space to beamspace. The resulting beamspace data vector is $\mathbf{y}(t) = \mathbf{F}_\mathbf{r}^H\mathbf{x}(t) = \mathbf{B}\mathbf{s}(t) + \mathbf{F}_\mathbf{r}^H\mathbf{n}(t)$, where $\mathbf{B} = \mathbf{F}_\mathbf{r}^H\underline{\mathbf{A}}$ is the *real-valued* beamspace DOA matrix having $\mathbf{b}(\boldsymbol{\theta}_i)$ of (18) as its columns. The corresponding beamspace covariance matrix is $\mathbf{R}_\mathbf{y} = \mathrm{E}[\mathbf{y}(t)\mathbf{y}^H(t)] = \mathbf{B}\mathbf{P}\mathbf{B}^T + \sigma\mathbf{I}$. The beamspace noise vector is white, due to orthogonality of $\mathbf{F}_\mathbf{r}^H$. Let $\mathbf{R} = \mathrm{Re}\{\mathbf{R}_\mathbf{y}\}$ denote the real part of the beamspace covariance matrix. We have

$$\mathbf{R} = \mathrm{Re}\{\mathbf{R}_\mathbf{y}\} = \mathbf{B}\mathbf{P}_R\mathbf{B}^T + \sigma\mathbf{I} \tag{19}$$

where $\mathbf{P}_R = \mathrm{Re}\{\mathbf{P}\}$. It is clear that the *real-valued* EVD of the matrix $\mathbf{R}$ yields bases for the beamspace signal and noise subspaces. Let $\mathbf{S}$ and $\mathbf{G}$ be orthonormal matrices that respectively span the beamspace signal and noise subspaces. We have

$$\mathbf{S} = [\mathbf{s}_1, \ldots, \mathbf{s}_d], \text{ and } \mathbf{G} = [\mathbf{g}_{d+1}, \ldots, \mathbf{g}_{M'}]. \tag{20}$$

The UCA-RB-MUSIC spectrum given by

$$S_b(\theta) = \frac{1}{\mathbf{b}^T(\theta)\mathbf{G}\mathbf{G}^T\mathbf{b}(\theta)} \propto \frac{1}{\mathbf{v}^H(\phi)\mathbf{J}_\zeta(\mathbf{W}\mathbf{G}\mathbf{G}^T\mathbf{W}^H)\mathbf{J}_\zeta\mathbf{v}(\phi)} \tag{21}$$

has peaks at $\boldsymbol{\theta} = \boldsymbol{\theta}_i$ corresponding to the signal arrival directions. Arrival angle estimates are therefore obtained by searching for d peaks in the 2-D UCA-RB-MUSIC spectrum of (21). Recapitulating, the UCA-RB-MUSIC algorithm requires a *real-valued* EVD of the matrix $\mathbf{R}$, and a 2-D search for peaks in the spectrum $S_b(\boldsymbol{\theta}) = S_b(\zeta, \phi)$. The elevation dependence of the spectrum is through the parameter $\zeta = k_0 r \sin\theta$, where θ is the elevation angle. It is clear from the above development that the omnidirectional element assumption can be relaxed. Both UCA-RB-MUSIC and UCA-ESPRIT can be employed if the element patterns are omnidirectional in azimuth (element gain depends only on elevation angle). The steps involved in the UCA-RB-MUSIC algorithm are summarized in Section IV, together with a summary of the UCA-ESPRIT algorithm.

C. Advantages of Phase Mode Excitation-Based Beamspace Processing

Beamspace operation with UCA's via phase mode excitation-based beamformers offers numerous advantages over element space operation. A major advantage of phase mode excitation-based beamforming is that it is the basis for the development of the attractive UCA-ESPRIT algorithm described in Section IV. The preceding development showed how UCA-RB-MUSIC requires only real-valued EVD's, as opposed to the complex-valued EVD's required for element space operation. Several other advantages such as improved estimator performance due to FB averaging, applicability of Root-MUSIC, ability to perform coarse searches of the UCA-RB-MUSIC spectrum via an FFT, and the ability to synthesize attractive azimuthal directional patterns are discussed below.

Forward/Backward Averaging in Beamspace: Forward/backward (FB) averaging [15] is a technique commonly employed with ULA's that exploits the centro-Hermitian property of the ULA manifold. FB averaging can improve the parameter estimation accuracy in correlated source scenarios. The beamformer $\mathbf{F}_\mathbf{e}^H$ synthesizes the centro-Hermitian beamspace manifold $\mathbf{a}_\mathbf{e}(\boldsymbol{\theta})$ of (12). FB averaging can therefore be applied in beamspace with UCA's. The FB averaged covariance matrix is $\mathbf{R}_{fb} = (\mathbf{R}_\mathbf{e} + \tilde{\mathbf{I}}\,\mathbf{R}_\mathbf{e}^*\tilde{\mathbf{I}})/2$, where $\mathbf{R}_\mathbf{e} = \mathbf{F}_\mathbf{e}^H\underline{\mathbf{R}}\mathbf{F}_\mathbf{e}$ is the beamspace covariance matrix under the beamformer $\mathbf{F}_\mathbf{e}^H$. It is easy to show [9] that the relationship $\mathbf{R} = \mathrm{Re}\{\mathbf{R}_\mathbf{y}\} = \mathbf{W}^H\mathbf{R}_{fb}\mathbf{W}$ holds when the beamformer $\mathbf{F}_\mathbf{r}^H$ is employed. This equation shows that UCA-RB-MUSIC effectively works with an FB averaged covariance matrix. Averaging similar to an FB average can be performed in element space with a UCA when the number of array elements N is even. This property does not appear to have been noticed or exploited prior to this work. Such averaging is possible because the permuted version $\mathbf{J}\underline{\mathbf{a}}(\theta)$ of the element space manifold vector with

$$\mathbf{J} = \begin{bmatrix} \mathbf{I}_{N/2} & \mathbf{0} \\ \mathbf{0} & \tilde{\mathbf{I}}_{N/2} \end{bmatrix}$$

is centro-Hermitian. FB type averaging *cannot*, however, be applied in element space when N is odd. Benefiting from the FB average, UCA-RB-MUSIC can outperform element space MUSIC for odd N, as demonstrated in Section VI.

Spectral Search via FFT: UCA-RB-MUSIC requires a search for peaks in the 2-D spectrum of (21) to obtain source azimuth and elevation estimates. This search is expedited by the fact that the computationally efficient FFT can be employed to evaluate the spectrum at each candidate elevation angle. Let $V(\phi;\zeta) = \mathbf{v}^H(\phi)\mathbf{J}_\zeta\mathbf{W}\mathbf{G}\mathbf{G}^T\mathbf{W}^H\mathbf{J}_\zeta\mathbf{v}(\phi)$ denote the UCA-RB-MUSIC null spectrum at the elevation specified by $\zeta = k_0 r\sin\theta$. With $\mathbf{Q}_\zeta = \mathbf{J}_\zeta\mathbf{W}\mathbf{G}\mathbf{G}^T\mathbf{W}^H\mathbf{J}_\zeta$, the null spectrum can be written in the form

$$V(\phi;\zeta) = \sum_{l=-(M'-1)}^{M'-1} a_\zeta(l)e^{jl\phi}$$

$$\text{where} \quad a_\zeta(l) = \sum_{i,j:j-i=l} \mathbf{Q}_\zeta(i,j). \tag{22}$$

The matrix $\mathbf{Q}_\zeta$ is Hermitian, such that $a_\zeta(-l) = a_\zeta^*(l)$. The null spectrum can thus be written in terms of the discrete time Fourier transform (DTFT) of the M' point sequence $a'_\zeta = \{a_\zeta(0), 2a_\zeta(-1), \ldots, 2a_\zeta(-M'+1)\}$. We have $A'_\zeta(\phi) = \sum_{l=0}^{M'-1} a'_\zeta(l)e^{-jl\phi}$ and $V(\phi;\zeta) = \mathrm{Re}\{A'_\zeta(\phi)\}$. The UCA-RB-MUSIC null spectrum $V(\phi;\zeta)$ at the elevation specified by ζ can thus be evaluated at L equispaced azimuth angles $\phi_l = 2\pi l/L, l = 0, 1, \ldots L-1$ via an L point FFT of the sequence a'_ζ, appropriately zero padded. The FFT cannot, however, be employed to facilitate the spectral search in element space.

Application of Root-MUSIC: The Root-MUSIC algorithm [16], originally developed for use in conjunction with ULA's, hinges on the Vandermonde structure of the ULA manifold. Root-MUSIC cannot be employed in element space with UCA's because the UCA manifold vectors $\underline{\mathbf{a}}(\theta)$ as given by (1) are not Vandermonde. Root-MUSIC can, however, be employed in beamspace to obtain azimuth angles of sources at a given elevation. This is because the azimuthal dependence of the UCA-RB-MUSIC null spectrum is through the vector $\mathbf{v}(\phi)$ of (13) that is Vandermonde, except for a multiplicative scale factor. The Root-MUSIC formulation follows from setting $z = e^{j\phi}$ in (22) and equating the null spectrum $V(\phi;\zeta)$ to 0. The polynomial equation

$$a_\zeta(M'-1)z^{2M'-2} + a_\zeta(M'-2)z^{2M'-3} + \cdots + a_\zeta(-M'+1) = 0$$

results. Roots z_i of this equation which are close to the unit circle yield the azimuth estimates $\phi_i = \arg(z_i)$ of sources at the elevation ζ. UCA-RB-MUSIC thus benefits from the concomitant advantages of Root-MUSIC, such as a lower failure rate for closely spaced sources at a given elevation.

Mapping onto ULA-Type Manifold: All of the advantages mentioned so far stem from the ULA-like structure of the vector $\mathbf{v}(\phi)$ in the beamspace manifolds of (12) and (16). Several researchers [3], [17] have considered the case where all incident sources are confined to a given elevation angle, say ζ_0, and the problem of interest is to estimate the source azimuth angles. It is clear from (12) that the beamformer $\mathbf{F}^H_{\zeta_0\mathrm{ULA}} = 1/\sqrt{N}\mathbf{J}^{-1}_{\zeta_0}\mathbf{F}^H_{\mathbf{e}}$ maps the UCA manifold $\underline{\mathbf{a}}(\zeta_0,\phi)$, corresponding to the elevation ζ_0, onto the manifold $\mathbf{v}(\phi)$ of (13). We have

$$\mathbf{F}^H_{\zeta_0\mathrm{ULA}}\underline{\mathbf{a}}(\zeta_0,\phi) = \mathbf{v}(\phi) \tag{23}$$

and the beamspace manifold corresponding to the elevation χ_0 is similar to that of a ULA. Employing the beamformer $\mathbf{F}^H_{\zeta_0\mathrm{ULA}}$ in this scenario thus allows *spatial smoothing* [15] to be applied in beamspace to combat the rank reducing effect caused by source coherency. In addition, sinc-type azimuthal patterns can be synthesized as with a ULA [18], [19], and the Beamspace Root-MUSIC algorithm [9] can therefore be employed. This algorithm provides azimuth estimates of sources in a given azimuthal sector via rooting of a reduced order polynomial.

Applicability to a UCA of Directional Elements: Phase mode excitation in conjunction with a UCA of directional elements yields far-field patterns similar in form to those of (8), corresponding to the omnidirectional element case. The only difference is that the mode amplitude is a sum of Bessel functions rather than just $J_m(\zeta)$ [20]. A beamspace version of MUSIC similar to UCA-RB-MUSIC can thus be developed for the UCA of directional elements. The algorithm employs the phase mode excitation beamformer $\mathbf{V}^H$ defined in (11). It possesses all the features of UCA-RB-MUSIC except that FB averaging is not possible, and that subspace estimates cannot be obtained via real-valued EVD's. Details are not provided due to space limitations.

D. Previous Work on the Application of ULA Techniques with UCA's

As stated in Section I, phase mode excitation-based beamformers have been employed to synthesize attractive directional patterns with UCA's, and obtain DOA estimates via the beamforming principle. Our initial investigations [18], [19] on phase mode excitation with UCA's focused on sinc-type pattern synthesis due to the similarity with ULA's. The only prior efforts on the application of ULA techniques with UCA's appear to be the work of Tewfik and Hong [21] and Friedlander [22].

To compare the present work with that of Tewfik and Hong, note that the vectors $\mathbf{w}_m^H$ defined in (4) are inverse DFT weight vectors. These vectors are used to construct the matrix $\mathbf{V}^H$ that defines the beamforming matrix $\mathbf{F}^H_{\mathbf{e}}$. Row $m \in [-M, M]$ of $\mathbf{V}^H$ excites the array with phase mode m, and a total of $M' = 2M+1 < N$ modes are excited. Thus, only M' of the N possible phase modes are excited. The reason for choosing $M' < N$ was to eliminate the residual contributions to the far-field pattern of (6), leading to a beamspace manifold whose azimuthal dependence was through the Vandermonde vector (except for a scalar multiplier) $\mathbf{v}(\phi)$. In [21], the authors employed a *full* $N \times N$ inverse DFT beamformer with the UCA. The residual terms consequently contributed significantly to some of the beams, thereby detracting from the Vandermonde structure. The approach proposed in [21] was to employ Root-MUSIC to obtain source azimuth estimates at each elevation angle under consideration. The imperfect Vandermonde structure, however, introduces errors in the estimates. The problem of elevation angle estimation was not addressed in [21].

Friedlander [22] proposed the interpolated array scheme that employed mapping matrices to map the manifold vectors for an arbitrary array onto Vandermonde ULA-type steering vectors. The azimuthal field of view corresponding to each candidate elevation angle was divided into sectors, for each of which a different mapping matrix had to be designed. The interpolating matrix for a given sector was computed as the least squares solution of an overdetermined system of equations corresponding to the desired mapping. The link between the present work and the interpolated array technique is provided by (23). It reveals that $\mathbf{F}^H_{\zeta_0\mathrm{ULA}}$ is the desired mapping matrix that maps the element space UCA manifold $\underline{\mathbf{a}}(\zeta_0,\phi)$, corresponding to the elevation ζ_0, onto the ULA-type manifold vector $\mathbf{v}(\phi)$. Phase mode analysis therefore provides closed form expressions for the mapping matrix for

each elevation, and the mapping is valid for the entire 360° of azimuth.

The UCA-ESPRIT algorithm described in the following section is an original technique for 2-D angle estimation with UCA's.

IV. The UCA-ESPRIT Algorithm

The UCA-ESPRIT algorithm developed in this section represents a significant advance in the area of 2-D arrival angle estimation. It is a *closed-form* algorithm, providing *automatically paired* source azimuth and elevation angle estimates. In contrast, the algorithms for 2-D arrival angle estimation to date have required expensive spectral searches [6], iterative solutions to multidimensional optimization problems [12], [13], or a pairing procedure for associating azimuth estimates with elevation estimates [11]. The UCA-ESPRIT algorithm is fundamentally different from ESPRIT in that it is not based on the displacement invariance array structure required by ESPRIT [7]. The development of UCA-ESPRIT hinges rather on a recursive relationship between Bessel functions. The steps in the algorithm, however, are similar to those of TLS ESPRIT [7]. The UCA-ESPRIT algorithm provides DOA estimates in closed-form via the eigenvalues of a matrix, as does ESPRIT in the 1-D angle estimation scenario. With UCA-ESPRIT, the eigenvalues have the form $\mu_i = \sin\theta_i e^{j\phi_i}$ and therefore provide automatically paired source azimuth and elevation angle estimates. Since $\theta_i \in [0, \pi/2]$, the eigenvalues satisfy $|\mu_i| \leq 1$, and lie within or on the unit circle. It is clear that $|\mu_i| = \sin\theta_i$, and $\arg(\mu_i) = \phi_i$, respectively, specify the elevation and azimuth angles of the ith source without ambiguity. Note also that $\mu_i = u_i + jv_i$, where $u_i = \sin\theta_i\cos\phi_i$ and $v_i = \sin\theta_i\sin\phi_i$, are the direction cosines with respect to the x and y axes, respectively. The u and v estimates are preferable to the θ and ϕ estimates when a source is close to boresight (elevation angle θ close to 0°). This is because azimuth is not very meaningful in such cases; for example, all azimuth angles are equivalent when $\theta = 0°$.

A phase mode excitation-based beamformer is employed to synthesize a beamspace manifold having the form required by UCA-ESPRIT. The beamformer that synthesizes this manifold is $\mathbf{F}_o^H = \mathbf{C_o}\mathbf{F}_e^H$, where $\mathbf{F}_e^H$ is as defined in (9), and

$$\mathbf{C_o} = \text{diag}\{(-1)^M, \ldots, (-1)^1, 1, 1, \ldots, 1\} \tag{24}$$

Comparison with (12) reveals that the beamspace manifold has the form

$$\mathbf{a_o}(\boldsymbol{\theta}) = \sqrt{N}\mathbf{J}_{\zeta_-}\mathbf{v}(\phi) \tag{25}$$

where $\mathbf{J}_{\zeta_-} = \text{diag}\{J_{-M}(\zeta), \ldots, J_{-1}(\zeta), J_0(\zeta), J_1(\zeta), \ldots, J_M(\zeta)\}$. Three vectors of size $M_e = M' - 2$ are extracted from the beamspace manifold as follows: $\mathbf{a}^{(i)} = \Delta^{(i)}\mathbf{a_o}(\theta)$, $i = -1, 0, 1$. The selection matrices $\Delta^{(-1)}, \Delta^{(0)}$ and $\Delta^{(1)}$ pick out the first, middle, and last M_e elements from $\mathbf{a_o}(\theta)$. The phases (excluding the signs of the values of the Bessel functions) of the vectors $\mathbf{a}^{(0)}, e^{j\phi}\mathbf{a}^{(-1)}$ and $e^{-j\phi}\mathbf{a}^{(1)}$ are the same. The recursive relationship $J_{m-1}(\zeta) + J_{m+1}(\zeta) = (2m/\zeta)J_m(\zeta)$ can now be applied to match the magnitude components of the three vectors. The resulting relationship is

$$\boldsymbol{\Gamma}\mathbf{a}^{(0)} = \mu\mathbf{a}^{(-1)} + \mu^*\mathbf{a}^{(1)} \tag{26}$$

where $\mu = \sin\theta e^{j\phi}$ and $\boldsymbol{\Gamma} = (\lambda/\pi r)\ \text{diag}\{-(M-1), \ldots, -1, 0, 1, \ldots, M-1\}$.

Let $\mathbf{A}_o = \mathbf{F}_o^H\underline{\mathbf{A}}$ denote the beamspace DOA matrix, and let $\mathbf{S_o}$ span $\mathcal{R}\{\mathbf{A_o}\}$. $\mathbf{S_o}$ can be obtained without performing a complex-valued EVD as follows. Employing the beamformer $\mathbf{F}_\mathbf{r}^H$ and performing the real-valued EVD of the matrix $\mathbf{R}$ of (19) yields the real matrix $\mathbf{S}$ that spans $\mathcal{R}\{\mathbf{B}\}$, such that $\mathbf{S} = \mathbf{BT}$, where $\mathbf{T}$ is a *real* nonsingular matrix. The equation $\mathbf{F}_\mathbf{o}^H = \mathbf{C_o}\mathbf{W}\mathbf{F}_\mathbf{r}^H$ relates the two beamformers. The matrix $\mathbf{C_o}\mathbf{W}$ is unitary and we therefore have $\mathbf{S_o} = \mathbf{C_o}\mathbf{W}\mathbf{S} = \mathbf{C_o}\mathbf{W}\mathbf{B}\mathbf{T} = \mathbf{A_o}\mathbf{T}$, as desired. The *real* matrix $\mathbf{T}$ therefore relates $\mathbf{S_o}$ and $\mathbf{A_o}$.

Now consider partitioning the DOA and subspace matrices as before, forming $\mathbf{A}^{(i)} = \Delta^{(i)}\mathbf{A_o}$ and $\mathbf{S}^{(i)} = \Delta^{(i)}\mathbf{S_o}$, $i = -1, 0, 1$. It is easy to verify the relationship $\mathbf{A}^{(1)} = \mathbf{D}\tilde{\mathbf{I}}\mathbf{A}^{(-1)^*}$, where $\mathbf{D} = \text{diag}\{(-1)^{M-2}, \ldots, (-1)^1, (-1)^0, (-1)^1, \ldots, (-1)^M\}$. The matrix $\mathbf{D}\tilde{\mathbf{I}}$ is unitary and is its own inverse. We have $\mathbf{S}^{(i)} = \mathbf{A}^{(i)}\mathbf{T}$, and this leads to $\mathbf{S}^{(1)} = \mathbf{D}\tilde{\mathbf{I}}\mathbf{S}^{(-1)^*}$, because $\mathbf{T}$ is real. Equation (26) now leads to the relationship $\boldsymbol{\Gamma}\mathbf{A}^{(0)} = \mathbf{A}^{(-1)}\boldsymbol{\Phi} + \mathbf{A}^{(1)}\boldsymbol{\Phi}^*$, where $\boldsymbol{\Phi} = \text{diag}\{\mu_1, \ldots, \mu_d\}$. Writing in terms of the signal subspace matrices, we have

$$\boldsymbol{\Gamma}\mathbf{S}^{(0)} = \mathbf{S}^{(-1)}\boldsymbol{\Psi} + \mathbf{D}\tilde{\mathbf{I}}\mathbf{S}^{(-1)^*}\boldsymbol{\Psi}^* \tag{27}$$

where $\boldsymbol{\Psi} = \mathbf{T}^{-1}\boldsymbol{\Phi}\mathbf{T}$. Rewriting this equation in block matrix form, we have

$$\mathbf{E}\underline{\boldsymbol{\Psi}} = \boldsymbol{\Gamma}\mathbf{S}^{(0)} \tag{28}$$

where $\mathbf{E} = [\mathbf{S}^{(-1)} \vdots \mathbf{D}\tilde{\mathbf{I}}\mathbf{S}^{(-1)^*}]$ and $\underline{\boldsymbol{\Psi}} = [\boldsymbol{\Psi}^T \vdots \boldsymbol{\Psi}^H]^T$. The system of (28) is overdetermined when $M_e = M' - 2 > 2d$ and has a unique solution $\underline{\boldsymbol{\Psi}}$ or, equivalently, $\boldsymbol{\Psi}$. Now $\boldsymbol{\Phi} = \mathbf{T}\bar{\boldsymbol{\Psi}}\mathbf{T}^{-1}$ and the eigenvalues of $\boldsymbol{\Psi}$ give the diagonal elements of $\boldsymbol{\Phi}$, which are $\mu_i = \sin\theta_i e^{j\phi_i}, i = 1, \ldots, d$. The eigenvalues of $\boldsymbol{\Psi}$ therefore yield automatically paired source azimuth and elevation angles. This procedure, however, fails when the system of (28) is underdetermined with $M_e < 2d$. This is because the system possesses infinite solutions having the block conjugate structure of $\underline{\boldsymbol{\Psi}}$, as will be shown subsequently. The maximum number of sources that UCA-ESPRIT can resolve is thus $d_{\max} = \lfloor M_e/2 \rfloor = M - 1$, a condition that is again reminiscent of ESPRIT.

Under noisy conditions, let $\hat{\mathbf{S}}^{(i)} = \Delta^{(i)}\hat{\mathbf{S}}_\mathbf{o}, i = -1, 0, 1$ be the signal subspace estimates. The subspace estimates can be shown to satisfy $\hat{\mathbf{S}}^{(1)} = \mathbf{D}\tilde{\mathbf{I}}\hat{\mathbf{S}}^{(-1)^*}$, as in the noiseless case. This relationship holds because the matrix $\hat{\mathbf{R}}$ whose EVD yields $\hat{\mathbf{S}}_\mathbf{o}$ is derived from an FB averaged covariance matrix. A detailed proof is not included due to space limitations. When $d < M_e/2$, $\hat{\underline{\boldsymbol{\Psi}}}$ can be obtained as the least squares solution to the system, corresponding to (28) for the noisy case. We have $\hat{\underline{\boldsymbol{\Psi}}} = (\hat{\mathbf{E}}^H\hat{\mathbf{E}})^{-1}\hat{\mathbf{E}}^H\boldsymbol{\Gamma}\hat{\mathbf{S}}^{(0)}$, where $\hat{\mathbf{E}} = [\hat{\mathbf{S}}^{(-1)} \vdots \mathbf{D}\tilde{\mathbf{I}}\hat{\mathbf{S}}^{(-1)^*}]$. The least squares solution has the desired block conjugate structure, with $\hat{\boldsymbol{\Psi}}$ and $\hat{\boldsymbol{\Psi}}^*$ being the upper and lower blocks of $\hat{\underline{\boldsymbol{\Psi}}}$, respectively. Source DOA estimates are obtained from eigenvalues of

$\hat{\mathbf{\Psi}}$, as in the noiseless case. The property $\mathbf{D\tilde{I}\Gamma\hat{S}}^{(0)} = \mathbf{\Gamma\hat{S}}^{(0)^*}$ is needed to prove that the least squares solution has block conjugate structure. Again, a detailed proof will not be provided. However, premultiplying (27) by $\mathbf{D\tilde{I}}$ shows that it holds in the noise-free case. The least squares solution can be written as two $d \times d$ coupled matrix equations. The above mentioned property shows that the right hand sides of these coupled equations are conjugates, thereby proving the block conjugate property. In addition, the two equations reduce to a single $d \times d$ complex matrix equation in $\hat{\mathbf{\Psi}}$ and $\hat{\mathbf{\Psi}}^*$. Consequently, the least squares solution $\hat{\mathbf{\Psi}}$ can be obtained via the solution of a system of $2d$ real equations. This reduces the required computation, as the normal procedure for obtaining the least squares solution involves solving a system of $2d$ complex equations.

Though UCA-ESPRIT provides DOA estimates in closed-form with relatively low computational effort, simulations performed in Section VI show that the UCA-RB-MUSIC estimator has lower variance than the UCA-ESPRIT estimator. The Newton iteration is a rapidly convergent, relatively low cost method for locating peaks in the UCA-RB-MUSIC spectrum. It, however, requires good initial values in the vicinity of the peak. UCA-ESPRIT provides good starting points for a Newton iteration. The performance of UCA-RB-MUSIC can, therefore, be realized if necessary at the additional cost of a Newton iteration. The algorithm summary below includes this option and effectively summarizes both UCA-ESPRIT and UCA-RB-MUSIC.

Algorithm Summary

1) Form the array sample covariance matrix $\hat{\underline{\mathbf{R}}} = \frac{1}{K}\sum_{t=1}^{K}\mathbf{x}(t)\mathbf{x}^H(t)$ by averaging over the K data snapshots. Also form the sample beamspace covariance matrix $\hat{\mathbf{R}}_\mathbf{y} = \mathbf{F}_\mathbf{r}^H\hat{\underline{\mathbf{R}}}\mathbf{F}_\mathbf{r}$.
2) Perform the *real-valued* EVD of the matrix $\hat{\mathbf{R}} = \mathrm{Re}\{\hat{\mathbf{R}}_\mathbf{y}\}$ and apply an appropriate detection technique to get an estimate $\hat{d}$ of the number of sources. Let the ordered eigenvalues of $\hat{\mathbf{R}}$ be $\hat{\lambda}_1 \geq \cdots \geq \hat{\lambda}_{M'}$, and the corresponding orthonormal eigenvectors be $\hat{\mathbf{s}}_1, \ldots, \hat{\mathbf{s}}_{\hat{d}}, \hat{\mathbf{g}}_{\hat{d}+1}, \ldots, \hat{\mathbf{g}}_{M'}$. Form the matrices $\hat{\mathbf{S}} = [\hat{\mathbf{s}}_1, \ldots, \hat{\mathbf{s}}_{\hat{d}}]$ and $\hat{\mathbf{G}} = [\hat{\mathbf{g}}_{\hat{d}+1}, \cdots, \hat{\mathbf{g}}_{M'}]$ that span the estimated signal and noise subspaces respectively.
3) Form $\hat{\mathbf{S}}_\mathbf{o} = \mathbf{C}_\mathbf{o}\mathbf{W}\hat{\mathbf{S}}$ and partition to obtain $\hat{\mathbf{S}}^{(i)} = \Delta^{(i)}\hat{\mathbf{S}}_\mathbf{o}$, $i = -1, 0$. Construct the matrix $\hat{\mathbf{E}} = [\hat{\mathbf{S}}^{(-1)} \vdots \mathbf{D\tilde{I}}\hat{\mathbf{S}}^{(-1)^*}]$.
4) Obtain $\hat{\mathbf{\Psi}}$ such that $\hat{\underline{\mathbf{\Psi}}}_{\mathrm{LS}} = [\hat{\mathbf{\Psi}}^T \vdots \hat{\mathbf{\Psi}}^H]^T$ is the least squares solution to $\hat{\mathbf{E}}\hat{\underline{\mathbf{\Psi}}} = \mathbf{\Gamma}\hat{\mathbf{S}}^{(0)}$. $\hat{\mathbf{\Psi}}$ can be obtained by solving a system of $2d$ real equations.
5) Compute the eigenvalues $\hat{\mu}_i$, $i = 1, \ldots, d$ of $\hat{\mathbf{\Psi}}$. The estimates of the elevation and azimuth angles of the ith source are $\hat{\theta}_i = \sin^{-1}(|\hat{\mu}_i|)$ and $\hat{\phi}_i = \arg(\hat{\mu}_i)$, respectively. If direction cosine estimates are desired, we have $\hat{u}_i = \mathrm{Re}\{\hat{\mu}_i\}$, and $\hat{v}_i = \mathrm{Im}\{\hat{\mu}_i\}$.
6) DOA estimates of lower variance can be obtained by using the UCA-ESPRIT estimates from step 5 as starting points for a Newton search for nearby maxima in the 2-D UCA-RB-MUSIC spectrum $\hat{S}_\mathrm{h}(\zeta, \phi) = 1/\mathbf{v}^H(\phi)\mathbf{J}_\zeta\mathbf{W}\hat{\mathbf{G}}\hat{\mathbf{G}}^T\mathbf{W}^H\mathbf{J}_\zeta\mathbf{v}(\phi)$. Again, $\zeta = k_0 r \sin\theta$.
7) As discussed in Section III, Root-MUSIC may be employed to resolve sources at a given elevation and closely spaced in azimuth even if the UCA-RB-MUSIC spectrum reveals only a single peak in the vicinity.

We now provide an outline of the proof that the system of (28) has an infinite number of solutions with the block conjugate structure of $\underline{\mathbf{\Psi}}$ when $M_e < 2d$. The system is underdetermined under the stated conditions and has infinite solutions. The pseudo right inverse gives the minimum norm solution $\underline{\mathbf{\Psi}}_{\mathrm{MIN}} = \mathbf{E}^H(\mathbf{E}\mathbf{E}^H)^{-1}\mathbf{\Gamma}\mathbf{S}^{(0)}$. As with the least squares solution in the overdetermined case, it can be shown that the minimum norm solution has block conjugate structure. We will show that the null space of $\mathbf{E}$ can be spanned by linearly independent block conjugate vectors. Linear combinations of these vectors in $\eta(\mathbf{E})$ can therefore be added to the columns of $\underline{\mathbf{\Psi}}_{\mathrm{MIN}}$ while retaining the block conjugate structure and satisfying (28). This proves that the solution $\mathbf{\Psi}$ to (27) is not unique. The following steps show how to construct block conjugate vectors in $\eta(\mathbf{E})$. Let $\mathbf{y} = [\mathbf{y}_1^T \vdots \mathbf{y}_2^T]^T \in \eta(\mathbf{E}) = \eta(\mathbf{E}^H\mathbf{E})$. It can be shown that the block conjugate vector $[(\mathbf{y}_1 + \mathbf{y}_2^*)^T \vdots (\mathbf{y}_1^* + \mathbf{y}_2)^T]^T \in \eta(\mathbf{E}^H\mathbf{E})$.

This completes the development of the UCA-ESPRIT algorithm. The performance analysis results in the following section are concerned with the asymptotic variances of MUSIC-type estimators for the case where the MUSIC spectrum is a function of *two variables*, azimuth and elevation. Performance analysis of the UCA-ESPRIT estimator will be considered in a subsequent paper.

V. Performance Analysis

Expressions for the variances-covariances of the MUSIC estimator when the MUSIC spectrum is a function of *one variable* are derived in [14]. Planar arrays provide azimuth and elevation estimates of sources, and the corresponding MUSIC spectrum is a function of *two variables*, as in (21). To our knowledge, asymptotic expressions for the variance of the MUSIC estimator in the 2-D angle estimation scenario are not available. In particular, variance results for the UCA-RB-MUSIC estimator that employs real-valued EVD's to obtain signal and noise subspace estimates are not available. Asymptotic expressions for the variance of the MUSIC estimator for the 2-D case (with arbitrary array configurations) are derived in this section. Variance expressions for the UCA-RB-MUSIC estimator that works with subspace estimates obtained via real-valued EVD's are also derived. Theorems 5.1 and 5.2 contain the main results; they respectively give asymptotic expressions for the variances of the element space MUSIC and UCA-RB-MUSIC estimators. Results on the Cramer–Rao bound (CRB) for the estimation problem are also presented.

Before going into the analysis, we restate some of the assumptions made, and introduce some notation. The number of incident signals d is assumed to be known. The signals $\mathbf{s}(t)$ and noises $\mathbf{n}(t)$ are assumed to be stationary, zero mean, uncorrelated random processes. The noise process $\mathbf{n}(t)$ is assumed to be complex Gaussian and spatially white with covariance matrix $\sigma\mathbf{I}$. The signals are assumed to be

noncoherent, and the source covariance matrix $\mathbf{P}$ is thus positive definite. The number of data snapshots is K, and the dimension of the data vectors (whether in element space or beamspace) is assumed to be N'. UCA-RB-MUSIC works with an EVD of the real matrix $\mathbf{R}$ of (19). The eigenvalues of $\mathbf{R}$ in descending order are $\{\lambda_i\}_{i=1}^{N'}$, and the real, orthonormal matrices $\mathbf{S}$ and $\mathbf{G}$ that, respectively, span the beamspace signal and noise subspaces are as defined in (20). Underbars are used to denote the quantities for the element space case, e.g., $\underline{\mathbf{G}}$ is the matrix spanning the element space noise subspace. Hats are used to denote estimates of quantities, e.g., $\hat{\mathbf{G}}$. As defined earlier, the UCA element space manifold is $\underline{\mathbf{a}}(\boldsymbol{\theta})$, and the beamspace manifold with UCA-RB-MUSIC is $\mathbf{b}(\boldsymbol{\theta})$. The source DOA's are represented by the vector $\boldsymbol{\theta} = (\zeta, \phi)$, where ϕ is the azimuth angle, and the elevation dependence is through $\zeta = k_0 r \sin\theta$. Finally, subscripts are used to denote partial derivatives, e.g., $\mathbf{b}_\zeta$ and $\mathbf{b}_{\zeta\phi}$ represent the first partial derivative of $\mathbf{b}$ with respect to ζ and the mixed partial derivative with respect to ζ and ϕ, respectively.

The following lemma gives asymptotic expressions (large number of snapshots K) for the MUSIC estimation errors. The results are based on a first-order Taylor expansion of the MUSIC null spectrum. Part a) of the lemma addresses the element space case and part b), the real beamspace case. This lemma is the first step in the estimator variance derivations. Part b) of the lemma is proved in Appendix A. The proof for part a) is similar, except for the fact that the manifold vectors and subspace matrices are complex-valued.

Lemma 5.1:

a) The asymptotic expression (large K) for the element space MUSIC estimation error vector for source i, $\underline{\mathbf{e}}_i = [(\underline{\hat{\zeta}}_i - \zeta_i), (\underline{\hat{\phi}}_i - \phi_i)]^T$ is

$$\underline{\mathbf{e}}_i = \{\underline{\mathbf{E}}^{-1}\underline{\mathbf{p}}\}_{\boldsymbol{\theta}=\boldsymbol{\theta}_i} \tag{29}$$

where

$$\underline{\mathbf{E}} = \begin{bmatrix} \underline{\mathbf{a}}_\zeta^H \underline{\mathbf{G}}\underline{\mathbf{G}}^H \underline{\mathbf{a}}_\zeta & \mathrm{Re}\{\underline{\mathbf{a}}_\phi^H \underline{\mathbf{G}}\underline{\mathbf{G}}^H \underline{\mathbf{a}}_\zeta\} \\ \mathrm{Re}\{\underline{\mathbf{a}}_\phi^H \underline{\mathbf{G}}\underline{\mathbf{G}}^H \underline{\mathbf{a}}_\zeta\} & \underline{\mathbf{a}}_\phi^H \underline{\mathbf{G}}\underline{\mathbf{G}}^H \underline{\mathbf{a}}_\phi \end{bmatrix} = \begin{bmatrix} \underline{a} & \underline{c} \\ \underline{c} & \underline{b} \end{bmatrix}$$

is a symmetric, positive definite matrix with determinant $\underline{\Delta}$. The vector

$$\underline{\mathbf{P}} = \begin{bmatrix} -\mathrm{Re}\{\underline{\mathbf{a}}^H \hat{\underline{\mathbf{G}}}\hat{\underline{\mathbf{G}}}^H \underline{\mathbf{a}}_\zeta\} \\ -\mathrm{Re}\{\underline{\mathbf{a}}^H \hat{\underline{\mathbf{G}}}\hat{\underline{\mathbf{G}}}^H \underline{\mathbf{a}}_\phi\} \end{bmatrix} = \begin{bmatrix} \underline{e} \\ \underline{f} \end{bmatrix}$$

is a random vector.

b) The asymptotic expression (large K) for the UCA-RB-MUSIC estimation error vector for source i, $\mathbf{e}_i = [(\hat{\zeta}_i - \zeta_i), (\hat{\phi}_i - \phi_i)]^T$ is

$$\mathbf{e}_i = \{\mathbf{E}^{-1}\mathbf{p}\}_{\boldsymbol{\theta}=\boldsymbol{\theta}_i} \tag{30}$$

where

$$\mathbf{E} = \begin{bmatrix} \mathbf{b}_\zeta^T \mathbf{G}\mathbf{G}^T \mathbf{b}_\zeta & \mathbf{b}_\phi^T \mathbf{G}\mathbf{G}^T \mathbf{b}_\zeta \\ \mathbf{b}_\phi^T \mathbf{G}\mathbf{G}^T \mathbf{b}_\zeta & \mathbf{b}_\phi^T \mathbf{G}\mathbf{G}^T \mathbf{b}_\phi \end{bmatrix} = \begin{bmatrix} a & c \\ c & b \end{bmatrix}$$

is a symmetric, positive definite matrix with determinant Δ. The vector

$$\mathbf{p} = \begin{bmatrix} -\mathbf{b}^T \hat{\mathbf{G}}\hat{\mathbf{G}}^T \mathbf{b}_\zeta \\ -\mathbf{b}^T \hat{\mathbf{G}}\hat{\mathbf{G}}^T \mathbf{b}_\phi \end{bmatrix} = \begin{bmatrix} e \\ f \end{bmatrix}$$

is a random vector.

The following lemma restates the well known result [14] on the statistics of the signal space eigenvectors of the sample covariance matrix $\hat{\underline{\mathbf{R}}}$ for the element space case. $\hat{\underline{\mathbf{R}}}$ is a complex Wishart distributed with K degrees of freedom.

Lemma 5.2: The estimation errors $(\hat{\underline{\mathbf{s}}}_i - \underline{\mathbf{s}}_i)$ for the element space case are asymptotically (for large K) jointly Gaussian distributed with zero means and covariance matrices given by

$$E[(\hat{\underline{\mathbf{s}}}_i - \underline{\mathbf{s}}_i)(\hat{\underline{\mathbf{s}}}_j - \underline{\mathbf{s}}_j)^H] = \frac{\underline{\lambda}_i}{K}\left[\sum_{\substack{r=1 \\ r\neq i}}^{d} \frac{\underline{\lambda}_r}{(\underline{\lambda}_r - \underline{\lambda}_i)^2}\underline{\mathbf{s}}_r\underline{\mathbf{s}}_r^H + \sum_{r=d+1}^{N'} \frac{\sigma}{(\underline{\lambda}_i - \sigma)^2}\underline{\mathbf{g}}_r\underline{\mathbf{g}}_r^H\right]\delta_{ij}. \tag{31}$$

The following theorem gives expressions for the variances of the element space MUSIC azimuth and elevation estimators; the results are applicable for arbitrary array configurations. The proof employs Lemmas 5.1 and 5.2, and is similar to the proof of Theorem 5.2 in Appendix B.

Theorem 5.1: The element space MUSIC estimation error vector for source i, $\underline{\mathbf{e}}_i = [(\underline{\hat{\zeta}}_i - \zeta_i), (\underline{\hat{\phi}}_i - \phi_i)]^T$ is asymptotically zero mean with covariance matrix

$$\mathrm{Cov}(\underline{\mathbf{e}}_i) = \begin{bmatrix} \mathrm{Var}\,\underline{\hat{\zeta}}_i & \mathrm{Cov}(\underline{\hat{\zeta}}_i, \underline{\hat{\phi}}_i) \\ \mathrm{Cov}(\underline{\hat{\zeta}}_i, \underline{\hat{\phi}}_i) & \mathrm{Var}\,\underline{\hat{\phi}}_i \end{bmatrix} = \frac{\sigma\underline{\rho}}{2K\underline{\Delta}}\begin{bmatrix} \underline{b} & \underline{c} \\ \underline{c} & \underline{a} \end{bmatrix}_{\boldsymbol{\theta}=\boldsymbol{\theta}_i}$$

where $\underline{a}$, $\underline{b}$, and $\underline{\Delta}$ are as defined in Lemma 5.1a). Two expressions for the factor $\underline{\rho}$ follow. The latter expression is useful for analytical studies of performance.

$$\underline{\rho}(\boldsymbol{\theta}_i) = \sum_{r=1}^{d} \frac{\underline{\lambda}_r}{(\underline{\lambda}_r - \sigma)^2}|\underline{\mathbf{a}}^H(\boldsymbol{\theta}_i)\underline{\mathbf{s}}_r|^2 = [\mathbf{P}^{-1}]_{ii} + \sigma\left[\mathbf{P}^{-1}(\underline{\mathbf{A}}^H\underline{\mathbf{A}})^{-1}\mathbf{P}^{-1}\right]_{ii}.$$

The following lemma, drawn from [23], gives the statistics of the signal space eigenvectors of the matrix $\hat{\mathbf{R}} = \mathrm{Re}\{\hat{\mathbf{R}}_\mathbf{y}\}$ employed by the UCA-RB-MUSIC algorithm. $\hat{\mathbf{R}}$ is derived from an FB averaged covariance matrix, and is not Wishart distributed. The signal eigenvector estimates are assumed to be normalized such that $\|\hat{\mathbf{s}}_i\| = 1, \hat{\mathbf{s}}_{ii} \geq 0$, and $\mathbf{s}_i^T\hat{\mathbf{s}}_i \geq 0$.

Lemma 5.3: The estimation errors $(\hat{\mathbf{s}}_i - \mathbf{s}_i)$ with UCA-RB-MUSIC are asymptotically (for large K) zero mean with covariance matrices given by

$$E[(\hat{\mathbf{s}}_i - \mathbf{s}_i)(\hat{\mathbf{s}}_j - \mathbf{s}_j)^T] = \frac{1}{K}\left[\sum_{\substack{r=1 \\ r\neq i}}^{d}\sum_{\substack{s=1 \\ s\neq j}}^{d} \frac{\Gamma_{rsji}}{(\lambda_i - \lambda_r)(\lambda_j - \lambda_s)}\mathbf{s}_r\mathbf{s}_s^T + \delta_{ij}\sum_{r=d+1}^{N'} \frac{\lambda_i\sigma}{2(\lambda_i - \sigma)^2}\mathbf{g}_r\mathbf{g}_r^T\right] \tag{32}$$

where

$$\Gamma_{rsji} = \frac{1}{2}\{\lambda_i\lambda_s\delta_{ij}\delta_{rs} + \lambda_i\lambda_j\delta_{is}\delta_{jr} + \mathbf{w}_r^T(\mathbf{s}_s\mathbf{s}_j^T + \mathbf{s}_j\mathbf{s}_s^T)\mathbf{w}_i\}$$

and $\mathbf{w}_i = \mathrm{Im}\,\{\mathbf{R}_\mathbf{y}\}\mathbf{s}_i$.

The following theorem gives expressions for the variances of the UCA-RB-MUSIC azimuth and elevation estimators. Due to the inherent FB average, the estimator variances depend only on the real part $\mathbf{P}_R$ of the source covariance matrix $\mathbf{P}$.

The decorrelating effect of the FB average allows UCA-RB-MUSIC to outperform element space MUSIC in correlated source scenarios when N is odd. The theorem is proved in Appendix B.

Theorem 5.2: The UCA-RB-MUSIC estimation error vector for source i, $\mathbf{e}_i = [(\hat{\zeta}_i - \zeta_i), (\hat{\phi}_i - \phi_i)]^T$ is asymptotically zero mean with variances given by

$$\mathrm{Cov}(\mathbf{e}_i) = \begin{bmatrix} \mathrm{Var}\,\hat{\zeta}_i & \mathrm{Cov}(\hat{\zeta}_i, \hat{\phi}_i) \\ \mathrm{Cov}(\hat{\zeta}_i, \hat{\phi}_i) & \mathrm{Var}\,\hat{\phi}_i \end{bmatrix} = \frac{\sigma\rho}{2K\Delta} \begin{bmatrix} b & c \\ c & a \end{bmatrix}_{\boldsymbol{\theta}=\boldsymbol{\theta}_i}$$

where a, b, and Δ are as defined in Lemma 5.1b. Two expressions for the factor ρ follow. In the latter expression, which is useful for analytical studies of performance, $\mathbf{P}_R = \mathrm{Re}\{\mathbf{P}\}$.

$$\rho(\boldsymbol{\theta}_i) = \sum_{r=1}^{d} \frac{\lambda_r}{(\lambda_r - \sigma)^2} |\mathbf{b}^T(\boldsymbol{\theta}_i)\mathbf{s}_r|^2$$
$$= \left[\mathbf{P}_R^{-1}\right]_{ii} + \sigma \left[\mathbf{P}_R^{-1}\left(\mathbf{B}^T\mathbf{B}\right)^{-1}\mathbf{P}_R^{-1}\right]_{ii}.$$

The following lemma gives the Cramer-Rao bound (CRB) on the covariance matrix of unbiased estimators of the parameter vector $\boldsymbol{\Theta} = [\zeta_1, \ldots, \zeta_d, \phi_1, \ldots, \phi_d]^T$. The CRB expression below is based on a random signal model, and is known as the unconditional or stochastic CRB. The result is a generalization of a similar result in [24] for the 1-D angle estimation problem. The symbol $\odot$ is used to denote the Hadamard or element-wise matrix product. We point out that the expression for the conditional or deterministic CRB can be obtained by making the substitution $\mathbf{P}' = \mathbf{P}$ in the lemma.

Lemma 5.4: The unconditional CRB for any unbiased estimator of $\boldsymbol{\Theta}$ is

$$\mathrm{CRB}(\boldsymbol{\Theta}) = \frac{\sigma}{2K}\left[\mathrm{Re}\{\mathbf{H} \odot \mathbf{P}_+^T\}\right]^{-1} \tag{33}$$

where

$$\mathbf{P}_+ = \begin{bmatrix} \mathbf{P}' & \mathbf{P}' \\ \mathbf{P}' & \mathbf{P}' \end{bmatrix} \text{ with } \mathbf{P}' = \mathbf{P}\underline{\mathbf{A}}^H\underline{\mathbf{R}}^{-1}\underline{\mathbf{A}}\mathbf{P},$$
$$\mathbf{H} = \mathbf{D}^H\left[I - \underline{\mathbf{A}}\left(\underline{\mathbf{A}}^H\underline{\mathbf{A}}\right)^{-1}\underline{\mathbf{A}}^H\right]\mathbf{D},$$
$$\text{and } \mathbf{D} = [\underline{\mathbf{a}}_\zeta(\boldsymbol{\theta}_1), \ldots, \underline{\mathbf{a}}_\zeta(\boldsymbol{\theta}_d), \underline{\mathbf{a}}_\phi(\boldsymbol{\theta}_1), \ldots, \underline{\mathbf{a}}_\phi(\boldsymbol{\theta}_d)].$$

The following section documents the results of computer simulations of the UCA-RB-MUSIC and UCA-ESPRIT algorithms. The DOA estimates are observed to have very low bias in the scenario considered. The comparisons made between the estimator performance and the CRB are thus meaningful.

VI. Simulation Results

A UCA of radius $r = \lambda$, with $M = 6$ being the maximum phase mode excited, was employed for the simulations. The number of array elements was chosen to be $N = 19$. We see from Table I that the maximum residual contribution is negligible with these array parameters. Two equipowered sources in the far field of the array with arrival angles given by $(\zeta_1, \phi_1) = (6, 90^\circ)$ and $(\zeta_2, \phi_2) = (4.844, 78^\circ)$ were simulated. When cophasal beamforming is employed to steer the array to one of the source locations, the gain at the other source location is approximately 3 dB below the maximum gain. The sources are thus spaced approximately half a 3-dB beamwidth apart with reference to the cophasal array pattern. The sources were highly correlated, with the correlation coefficient referred to the center of the array being $0.9e^{j\pi/4}$. The number of snapshots was $K = 64$ and sample statistics were computed from 200 independent trials. For the simulations, the number of sources was assumed to be known. Also, the SNR's quoted are per source per array element.

The theoretical asymptotic (number of snapshots) performance curves for sources 1 and 2 are plotted in Figs. 3(a) and 4(a), respectively. The theoretical performance of element space MUSIC and UCA-RB-MUSIC, as predicted by Theorems 5.1 and 5.2, are plotted versus the SNR. The ultimate performance of the CRB as given by Lemma 5.4 is also plotted. The graphs show that UCA-RB-MUSIC indeed outperforms element space MUSIC. We also note that the UCA-RB-MUSIC performance is fairly close to the CRB despite the fact that the sources are highly correlated.

The sample standard deviations of the DOA estimates for sources 1 and 2 are plotted in Figs. 3(b) and 4(b), respectively. The dashed line once again depicts the theoretical performance of UCA-RB-MUSIC. The simulation results are seen to be in close agreement with the theoretical performance predictions, and thus validate the analysis of Section V. Localized iterative Newton searches were employed to obtain the UCA-RB-MUSIC estimates. The graphs also show that the UCA-RB-MUSIC estimates perform significantly better than the UCA-ESPRIT estimates, especially at low SNR's. As mentioned in the Algorithm Summary of Section IV, the UCA-ESPRIT estimates provide good starting points for localized Newton searches of the UCA-RB-MUSIC spectrum. The eigenvalues that directly give the DOA estimates with the UCA-ESPRIT algorithm are marked by "x's" in Fig. 5. The results of 200 runs at an SNR of 10 dB were superimposed to produce the figure. The true elevation angles are indicated by the dashed circles.

Graphs of the sample biases have not been plotted. The sample biases for source 1 corresponding to the SNR 0 dB are listed below to provide a feeling for the magnitude of the bias. The sample biases for the estimates of $\sin(\theta_1)$ from the UCA-RB-MUSIC and UCA-ESPRIT algorithms are, respectively, -0.013 and -0.027. The biases for the estimates of ϕ_1, ordered in similar fashion, are -0.012 and -0.014. The UCA-RB-MUSIC estimates are seen to have a lower bias than the UCA-ESPRIT estimates.

VII. Conclusion

This paper documents the development of two eigenstructure-based algorithms for 2-D angle estimation with UCA's. The first, UCA-RB-MUSIC, is a beamspace version of MUSIC that is characterized by a beamspace manifold whose form is similar to the ULA manifold. Techniques such as FB averaging, signal eigenvector estimation via real-valued EVD's, Root-MUSIC, and spatial smoothing that were developed for ULA's can thus be employed in beamspace with UCA's. Such techniques cannot be employed with the UCA in element space, and UCA-RB-MUSIC is thus superior to element space MUSIC in many respects. The second algorithm, UCA-ESPRIT, is the only available

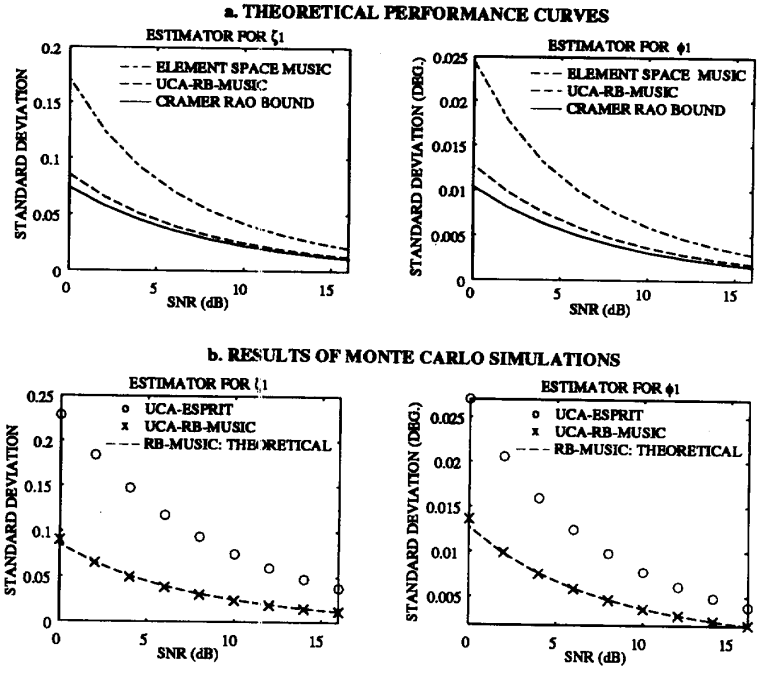

Fig. 3. Theoretical and experimental results for the first source.

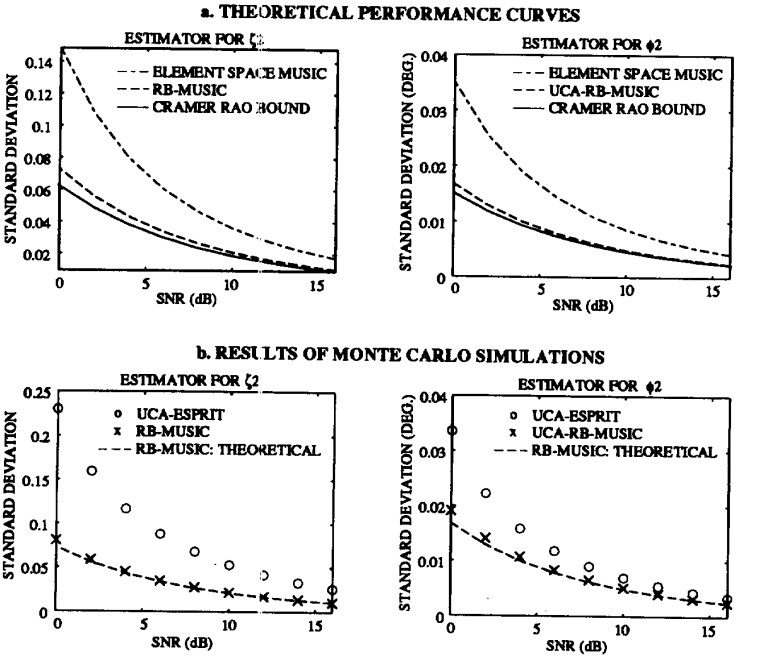

Fig. 4. Theoretical and experimental results for the second source.

closed-form algorithm for 2-D angle estimation, and thus represents a significant advance in the area. UCA-ESPRIT provides *automatically paired* source DOA estimates via the eigenvalues of the matrix Ψ that is obtained from the least squares solution to an overdetermined system of equations. UCA-ESPRIT requires less computation than existing 2-D angle estimation algorithms as expensive search procedures are not required, and signal subspace estimates can be obtained via real-valued EVD's. Results on the asymptotic performance of the UCA-RB-MUSIC and element space

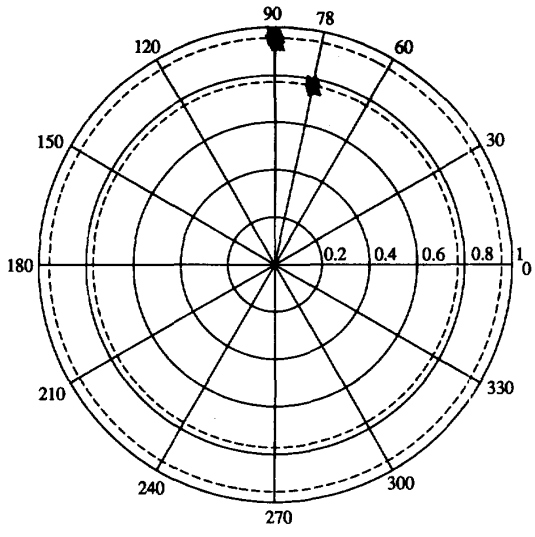

Fig. 5. Plot of UCA-ESPRIT eigenvalues.

MUSIC estimators for 2-D angle estimation are derived. Prior to this work, the performance of MUSIC had been examined for only the 1-D angle estimation problem. Computer simulations that demonstrate the efficacy of the algorithms and validate the performance analysis results are presented.

Appendix A
Proof of Lemma 5.1b

The UCA-RB-MUSIC null spectrum is $V(\boldsymbol{\theta}) = \mathbf{b}^T(\boldsymbol{\theta})\hat{\mathbf{G}}\hat{\mathbf{G}}^T\mathbf{b}(\boldsymbol{\theta})$. The null spectrum has a local minimum at $\hat{\boldsymbol{\theta}}_i = (\hat{\zeta}_i, \hat{\phi}_i)$, and we therefore have $V_\zeta(\hat{\boldsymbol{\theta}}_i) = 0$, and $V_\phi(\hat{\boldsymbol{\theta}}_i) = 0$. Because $\hat{\boldsymbol{\theta}}_i$ is a consistent estimator of $\boldsymbol{\theta}_i$, we obtain the following equations from first order Taylor series expansions.

$$0 = V_\zeta(\hat{\boldsymbol{\theta}}_i) \approx V_\zeta(\boldsymbol{\theta}_i) + V_{\zeta\zeta}(\boldsymbol{\theta}_i)(\hat{\zeta}_i - \zeta_i) + V_{\zeta\phi}(\boldsymbol{\theta}_i)(\hat{\phi}_i - \phi_i)$$
$$0 = V_\phi(\hat{\boldsymbol{\theta}}_i) \approx V_\phi(\boldsymbol{\theta}_i) + V_{\phi\zeta}(\boldsymbol{\theta}_i)(\hat{\zeta}_i - \zeta_i) + V_{\phi\phi}(\boldsymbol{\theta}_i)(\hat{\phi}_i - \phi_i)$$

Putting these equations into matrix form, we get

$$\begin{bmatrix} V_{\zeta\zeta}(\boldsymbol{\theta}_i) & V_{\zeta\phi}(\boldsymbol{\theta}_i) \\ V_{\phi\zeta}(\boldsymbol{\theta}_i) & V_{\phi\phi}(\boldsymbol{\theta}_i) \end{bmatrix} \begin{bmatrix} (\hat{\zeta}_i - \zeta_i) \\ (\hat{\phi}_i - \phi_i) \end{bmatrix} = -\begin{bmatrix} V_\zeta(\boldsymbol{\theta}_i) \\ V_\phi(\boldsymbol{\theta}_i) \end{bmatrix}. \quad (34)$$

The expansions for the derivatives occurring in this equation are as given below. Only terms which result in contributions of order $O(1/N)$ in (34) are retained.

$$\begin{aligned} V_\zeta(\boldsymbol{\theta}_i) &= 2\mathbf{b}^T(\boldsymbol{\theta}_i)\hat{\mathbf{G}}\hat{\mathbf{G}}^T\mathbf{b}_\zeta(\boldsymbol{\theta}_i) \\ V_\phi(\boldsymbol{\theta}_i) &= 2\mathbf{b}^T(\boldsymbol{\theta}_i)\hat{\mathbf{G}}\hat{\mathbf{G}}^T\mathbf{b}_\phi(\boldsymbol{\theta}_i) \\ V_{\zeta\zeta}(\boldsymbol{\theta}_i) &= 2\mathbf{b}_\zeta^T(\boldsymbol{\theta}_i)\hat{\mathbf{G}}\hat{\mathbf{G}}^T\mathbf{b}_\zeta(\boldsymbol{\theta}_i) + 2\mathbf{b}^T(\boldsymbol{\theta}_i)\hat{\mathbf{G}}\hat{\mathbf{G}}^T\mathbf{b}_{\zeta\zeta}(\boldsymbol{\theta}_i) \\ &\approx 2\mathbf{b}_\zeta^T(\boldsymbol{\theta}_i)\mathbf{G}\mathbf{G}^T\mathbf{b}_\zeta(\boldsymbol{\theta}_i) \\ V_{\phi\phi}(\boldsymbol{\theta}_i) &= 2\mathbf{b}_\phi^T(\boldsymbol{\theta}_i)\hat{\mathbf{G}}\hat{\mathbf{G}}^T\mathbf{b}_\phi(\boldsymbol{\theta}_i) + 2\mathbf{b}^T(\boldsymbol{\theta}_i)\hat{\mathbf{G}}\hat{\mathbf{G}}^T\mathbf{b}_{\phi\phi}(\boldsymbol{\theta}_i) \\ &\approx 2\mathbf{b}_\phi^T(\boldsymbol{\theta}_i)\mathbf{G}\mathbf{G}^T\mathbf{b}_\phi(\boldsymbol{\theta}_i) \\ V_{\zeta\phi}(\boldsymbol{\theta}_i) &= 2\mathbf{b}_\phi^T(\boldsymbol{\theta}_i)\hat{\mathbf{G}}\hat{\mathbf{G}}^T\mathbf{b}_\zeta(\boldsymbol{\theta}_i) + 2\mathbf{b}^T(\boldsymbol{\theta}_i)\hat{\mathbf{G}}\hat{\mathbf{G}}^T\mathbf{b}_{\zeta\phi}(\boldsymbol{\theta}_i) \\ &= V_{\phi\zeta}(\boldsymbol{\theta}_i) \\ &\approx 2\mathbf{b}_\phi^T(\boldsymbol{\theta}_i)\mathbf{G}\mathbf{G}^T\mathbf{b}_\zeta(\boldsymbol{\theta}_i) \end{aligned}$$

Substituting these expressions back into (34) and dropping the common factor of two leads to the desired result $\mathbf{E}\mathbf{e}_i = \mathbf{p}$, where $\mathbf{E}$, $\mathbf{e}_i$, and $\mathbf{p}$ are as defined in the lemma. Positive definitiveness and hence nonsingularity of $\mathbf{E}$ follow from the Cauchy–Schwarz inequality.

Appendix B
Proof of Theorem 5.2

The MUSIC estimation error vector as given by Lemma 5.1b is

$$\mathbf{e}_i = \begin{bmatrix} \hat{\zeta}_i - \zeta_i \\ \hat{\phi}_i - \phi_i \end{bmatrix} = \{\mathbf{E}^{-1}\mathbf{p}\}_{\boldsymbol{\theta}=\boldsymbol{\theta}_i} = \frac{1}{\Delta}\begin{bmatrix} b & -c \\ -c & a \end{bmatrix}\begin{bmatrix} e \\ f \end{bmatrix}.$$

We proceed to derive the expression for the variance of the estimator $\hat{\zeta}_i$. The remaining results can be obtained in similar fashion. The above equation yields

$$\hat{\zeta}_i - \zeta_i = \frac{b'}{\Delta}, \text{ where } b' = be - cf. \quad (35)$$

As shown in [14], we have $\mathbf{b}^T(\boldsymbol{\theta}_i)\hat{\mathbf{G}}\hat{\mathbf{G}}^T \approx -\mathbf{b}^T(\boldsymbol{\theta}_i)\mathbf{S}\hat{\mathbf{S}}^T\mathbf{G}\mathbf{G}^T$. This result leads to the following expressions for the random quantities e and f in terms of the estimated signal space eigenvectors, whose statistics are available. The dependence of the expressions on $\boldsymbol{\theta}_i$ is dropped for conciseness.

$$e = -\mathbf{b}^T\hat{\mathbf{G}}\hat{\mathbf{G}}^T\mathbf{b}_\zeta \approx \mathbf{b}^T\mathbf{S}\hat{\mathbf{S}}^T\mathbf{G}\mathbf{G}^T\mathbf{b}_\zeta = \mathbf{b}_\zeta^T\mathbf{G}\mathbf{G}^T\hat{\mathbf{S}}\mathbf{S}^T\mathbf{b}$$
$$f = -\mathbf{b}^T\hat{\mathbf{G}}\hat{\mathbf{G}}^T\mathbf{b}_\phi \approx \mathbf{b}^T\mathbf{S}\hat{\mathbf{S}}^T\mathbf{G}\mathbf{G}^T\mathbf{b}_\phi = \mathbf{b}_\phi^T\mathbf{G}\mathbf{G}^T\hat{\mathbf{S}}\mathbf{S}^T\mathbf{b}$$

Substituting in (35), and using the definitions in Lemma 5.1b, leads to the following expression for the term b':

$$b' = q_1^T\mathbf{z}, \quad (36)$$

where $q_1 = (b\mathbf{b}_\zeta - c\mathbf{b}_\phi)$ is a deterministic quantity, and $\mathbf{z} = \mathbf{G}\mathbf{G}^T\hat{\mathbf{S}}\mathbf{S}^T\mathbf{b}$ is a random vector. The vector $\mathbf{z}$ will shortly be shown to have the following statistics:

$$E\mathbf{z} = 0,$$
$$\text{and } \mathrm{Cov}\mathbf{z} = E\mathbf{z}\mathbf{z}^T = \frac{\sigma\rho}{2K}\mathbf{G}\mathbf{G}^T \quad (37)$$

where $\rho(\boldsymbol{\theta}_i)$ is defined in the theorem statement. Equation 36 now yields $\mathrm{E}b' = 0$ and $\mathrm{Var}b' = \frac{\sigma\rho}{2K}q_1^T\mathbf{G}\mathbf{G}^Tq_1 = \frac{\sigma\rho\Delta b}{2K}$. The final equality results because $q_1^T\mathbf{G}\mathbf{G}^Tq_1 = \Delta b$, a relationship which is easily verified. Employing these results in (35) yields the desired results. We obtain $E(\hat{\zeta}_i - \zeta_i) = 0$, and $\mathrm{Var}\hat{\zeta}_i = \frac{\sigma}{2K}\left\{\frac{\rho b}{\Delta}\right\}_{\theta=\theta_i}$. The proof for the expression of $\rho(\boldsymbol{\theta}_i)$ in terms of $\mathbf{P}_R = \mathrm{Re}\{\mathbf{P}\}$, where $\mathbf{P}$ is the source covariance matrix, follows a similar proof in [14].

It now remains to verify the expressions for the statistics of the vector $\mathbf{z}$. We have

$$\mathbf{z} = \mathbf{G}\mathbf{G}^T\hat{\mathbf{S}}\mathbf{S}^T\mathbf{b} = \sum_{k=1}^{d}\mathbf{G}\mathbf{G}^T\hat{\mathbf{s}}_k(\mathbf{s}_k^T\mathbf{b})$$
$$= \sum_{k=1}^{d}(\mathbf{b}^T\mathbf{s}_k)\mathbf{G}\mathbf{G}^T(\hat{\mathbf{s}}_k - \mathbf{s}_k). \quad (38)$$

We have $E(\hat{\mathbf{s}}_k - \mathbf{s}_k) = 0$ from Lemma 5.3, and thus $E\mathbf{z} = 0$ as claimed. Now,

$$\begin{aligned}\text{Cov}\mathbf{z} &= E[\mathbf{z}\mathbf{z}^T] \\ &= \sum_{k=1}^{d}\sum_{l=1}^{d}(\mathbf{b}^T\mathbf{s}_k)(\mathbf{b}^T\mathbf{s}_l)\mathbf{G}\mathbf{G}^T \\ &\qquad \times E\left[(\hat{\mathbf{s}}_k - \mathbf{s}_k)(\hat{\mathbf{s}}_l - \mathbf{s}_l)^T\right]\mathbf{G}\mathbf{G}^T.\end{aligned}$$

Using the result of Lemma 5.3 on the signal e genvector statistics, we obtain

$$\begin{aligned}\text{Cov}\mathbf{z} &= \frac{1}{K}\sum_{k=1}^{d}\sum_{l=1}^{d}(\mathbf{b}^T\mathbf{s}_k)(\mathbf{b}^T\mathbf{s}_l)\frac{\lambda_k\sigma\delta_{kl}}{2(\lambda_k-\sigma)^2}\sum_{r=d+1}^{N}\mathbf{g}_r\mathbf{g}_r^T \\ &= \frac{\sigma}{2K}\left(\sum_{k=1}^{d}\frac{\lambda_k}{(\lambda_k-\sigma)^2}|\mathbf{b}^T(\theta_i)\mathbf{s}_k|^2\right)\mathbf{G}\mathbf{G}^T \\ &= \frac{\sigma\rho(\theta_i)}{2K}\mathbf{G}\mathbf{G}^T\end{aligned}$$

as claimed in (37).

REFERENCES

[1] J. D. Tillman, C. E. Hickman, and H. P. Neff, "The theory of a single ring circular array," *Trans. Amer. Inst. Elect. Eng.*, vol. 80, pt. 1, p. 110, 1961.

[2] I. D. Longstaff, P. E. K. Chow, and D. E. N. Davies, "Directional properties of circular arrays," *Proc. Inst. Elec. Eng.*, vol. 114, June 1967.

[3] D. E. N. Davies, *The Handbook of Antenna Design* (A. W. Rudge *et al.*, Eds.). London: Peregrinus, 1983, vol. 2, chap. 12.

[4] ——, "A transformation between the phasing techniques required for linear and circular aerial arrays," *Proc. Inst. Elec. Eng.*, vol. 112, pp. 2041–2045, Nov. 1965.

[5] J. R. F. Guy and D. E. N. Davies, "UHF circular array incorporating open-loop null steering for communications," *Proc. Inst. Elec. Eng.*, pts. F and H, vol. 130, pp. 67–77, Feb. 1983.

[6] R. O. Schmidt, "Multiple emitter location and signal parameter estimation," *IEEE Trans. Antenn. Propagat.*, vol. AP-34, pp. 276–280, Mar. 1986.

[7] R. Roy and T. Kailath, "ESPRIT-Estimation of signal parameters via rotational invariance techniques," *IEEE Trans. Acoust., Speech, Signal Processing*, vol. 37, pp. 984–995, July 1989.

[8] A. Swindlehurst, "DOA identifiability for rotationally invariant arrays," *IEEE Trans. Acoust., Speech, Signal Processing*, vol. 40, pp. 1825–1828, July 1992.

[9] M. D. Zoltowski, G. M. Kautz, and S. D. Silverstein, "Beamspace Root-MUSIC," *IEEE Trans. Signal Processing*, vol. 41, pp. 344–364, Jan. 1993.

[10] P. Stoica and A. Nehorai, "Comparative performance of element-space and beam-space MUSIC estimators," *Circuits, Syst. Signal Processing*, vol. 10, pp. 285–292, 1991.

[11] M. D. Zoltowski and D. Stavrinides, "Sensor array signal processing via a Procrustes rotations based eigenanalysis of the ESPRIT data pencil," *IEEE Trans. Acoust., Speech, Signal Processing*, vol. 37, pp. 832–861, June 1989.

[12] A. L. Swindlehurst and T. Kailath, "Azimuth/Elevation direction finding using regular array geometries," *IEEE Trans. Aerosp. Electron. Syst.*, vol. 29, pp. 145–156, Jan. 1993.

[13] M. P. Clark and L. L. Scharf, "A maximum likelihood estimation technique for spatial-temporal modal analysis," *in Proc. Asilomar Conf. Signals, Syst., Comput.*, 1991, vol. 1, pp. 257–261.

[14] P. Stoica and A. Nehorai, "MUSIC, maximum likelihood and Cramer–Rao bound," *IEEE Trans. Acoust., Speech, Signal Processing*, vol. 37, pp. 720–741, May 1989.

[15] S. U. Pillai and B. H. Kwon, "Forward/backward spatial smoothing techniques for coherent signal identification," *IEEE Trans. Acoust., Speech, Signal Processing*, vol. 37, pp 8–15, Jan. 1989.

[16] A. J. Barabell, "Improving the resolution performance of eigenstructure-based direction-finding algorithms," *in Proc. IEEE Int. Conf. Acoust., Speech, Signal Processing* 1983, pp. 336–339.

[17] E. Doron and M. Doron, "Coherent wideband array processing," in *Proc. IEEE Int. Conf. Acoust., Speech, Signal Processing*, 1992, vol. 2, pp. 497–500.

[18] M. D. Zoltowski and C. P. Mathews, "Direction finding with uniform circular arrays via phase mode excitation and Beamspace Root-MUSIC," in *Proc. IEEE Int. Conf. Acoust., Speech, Signal Processing*, 1992, vol. 5, pp. 245–248.

[19] C. P. Mathews and M. D. Zoltowski, "Direction finding with circular arrays via phase mode excitation and Root-MUSIC," in *Proc. IEEE AP-S Int. Symp.*, 1992, vol. 2, pp. 1019–1022.

[20] T. Rahim and D. E. N. Davies, "Effect of directional elements on the directional response of circular antenna arrays," *Proc. Inst. Elec. Eng.*, pt. H, vol. 129, pp. 180–22, Feb. 1982.

[21] A. H. Tewfik and W. Hong, "On the application of uniform linear array bearing estimation techniques to uniform circular arrays," *IEEE Trans. Signal Processing*, vol. 40, pp. 1008–1011, Apr. 1992.

[22] B. Friedlander and A. J. Weiss, "Direction finding using spatial smoothing with interpolated arrays," *IEEE Trans. Aerosp. Electron. Syst.*, vol. 28, pp. 574–587, Apr. 1992.

[23] M. D. Zoltowski and G. M. Kautz, "Performance analysis of eigenstructure based DOA estimators employing conjugate centro-symmetric beamformers," in *Proc. 6th SSAP Workshop Stat. Signal Array Processing*, Oct. 1992, pp. 384–387.

[24] P. Stoica and A. Nehorai, "Performance study of conditional and unconditional direction-of-arrival estimation," *IEEE Trans. Acoust., Speech, Signal Processing*, vol. 38, pp. 1783–1795, Oct. 1990.

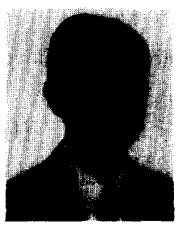

Cherian P. Mathews (M'93) was born in Madras, India, on October 26, 1966. He received the B.E. degree in electrical and electronics engineering from Anna University, Madras, in 1987, and the M.S. and Ph.D. degrees in electrical engineering from Purdue University, West Lafayette, IN, in 1989 and 1993, respectively.

He was awarded a Purdue University dissertation fellowship in 1993. He is currently a Visiting Assistant Professor at Purdue University. He is a contributing author to *Advances in Spectrum Analysis and Array Processing, Vol. III* (Prentice-Hall, 1994). His current research interests are in sensor array signal processing for radar and mobile communications.

Michael D. Zoltowski (S'79–M'86) was born in Philadelphia, PA on August 12, 1960. He received both the B.S. and M.S. degrees in electrical engineering with highest honors from Drexel University in 1983 and the Ph.D. degree in systems engineering from the University of Pennsylvania in 1986.

From 1982 to 1986, he was an Office of Naval Research Graduate Fellow. In conjunction with this fellowship, he held a visiting research position at the Naval Research Laboratory in Washington, DC, during Summer 1986. In Fall 1986, he joined the faculty of Purdue University, where he currently holds the position of Associate Professor of Electrical Engineering. In this capacity, he was the recipient of the IEEE Outstanding Branch Counselor/Advisor Award for 1989–1990 and the Ruth and Joel Spira Outstanding Teacher Award for 1990–1991. During 1987, he was a Summer Faculty Research Fellow at the Naval Ocean Systems Center in San Diego, CA.

Dr. Zoltowski was the recipient of the IEEE Signal Processing Society's 1991 Paper Award (Statistical Signal and Array Processing Technical Area). He is a contributing author to *Adaptive Radar Detection and Estimation* (Wiley, 1991) and *Advances in Spectrum Analysis and Array Processing, Vol. III* (Prentice-Hall, 1994). He has served as a consultant to the General Electric Company. His present research interests include sensor array signal processing for mobile communications, radar, and noncooperative electronic communications, adaptive beamforming, and higher order spectral analysis.